

# The mid-Pleistocene transition:

An Eastern Mediterranean perspective

Master thesis by Arno Dols

Utrecht University

Faculty of Geosciences

Department of Earth Sciences

1<sup>st</sup> Supervisor: prof. dr. Lucas Lourens

2<sup>nd</sup> Supervisor: Msc. Theodoor Konijnendijk



## Abstract

A reliable timescale is a critical tool in determining phase relations and causal relations in paleoclimate records. Presented here are oxygen isotope records collected from ODP site 967 located in the Eastern Mediterranean. The studied interval covers the MPT, from 1200 ka to 600 ka. Age control is provided by a Ti/Al timescale and changes that occur in global and local, Mediterranean, climate will be described based on this age model. New insights in the phase relation between orbital forcing and paleoclimate are gained by using this Ti/Al timescale.

A comparison of the benthic record based on a Ti/Al age model used in this study to the widely used Lisiecki and Raymo (2005) LR04 benthic stacked record reveals a good match between the two records. Although there are differences between the two benthic records they are in sync with regard to the major climatic transitions in the isotope records for most of the studied interval. The assumptions made by Lisiecki and Raymo in the tuning of their record such as lag of ice sheets, with regard to the astronomical cycles which govern their waxing and waning, concur with the Ti/Al age model used to date the isotope record of ODP site 967. The main differences which exist between both records are likely related to regional effects acting on the record of ODP site 967 since they are amplitude differences and usually not phase related.

An initial attempt at the establishment of a 100 ky period around 1200 ka was found, a precursor to the establishment of a 100 ky climate cycle. The influence of precession on glacial termination increases at this time. High precession amplitude, at high eccentricity, in combination with high obliquity result in a  $\sim 100$  ky period early in the MPT. The volume of ice formed during glacials in this early 100 ky regime did not significantly change from glacials ice volume before the MPT. This suggests a change in ice sheet dynamics, which requires a higher insolation maximum to melt completely.

Around 900 ka ice volume grows significantly, the changes in ice sheet dynamics may have altered the ice sheets to an extent where they become almost impervious to weak insolation maxima. This is seen in the suppression of obliquity maxima, which started at MIS 33. After the increase in ice volume around 900 ka the

skipping of obliquity maxima, instead of suppression, describes the trend seen in our benthic isotope record.

A fundamental change in ice sheet dynamics based on the regolith hypothesis is proposed. The increased sensitivity to high precession forcing in combination to obliquity is characteristic for the ice sheets which develop at the start of the MPT, a trend which continues over the MPT. The changes in ice sheet dynamics eventually result in larger glacial ice volume. The greater ice volume becomes even less sensitive to obliquity forcing. Glacial terminations occur only when the ice sheets have grown to an unstable size, over two obliquity cycles at high precession forcing.

# 1. Introduction

From the Oligocene onwards the global climate has undergone a series of major changes which resulted in the “100,000 year” ice age world we live in today. Significant glaciation on the Antarctic continent started 34 million years ago (Ma) (Zachos et al 2001; Coxall et al., 2005). Although there was glaciation on the Northern Hemisphere before 2.5 Ma the much larger ice caps started to form around the arctic at that time (Maslin et al., 1998). The further trend toward heavier  $\delta^{18}\text{O}$  isotope values, a proxy for climate, has been recorded globally following the Plio-Pleistocene transition around 2.5 Ma. The heavier  $\delta^{18}\text{O}$  values recorded in benthic oxygen isotope records are in part caused by the increased size of Northern Hemisphere ice sheets and in part by the decrease in deep ocean water temperature. Therefore the inception of large Northern Hemisphere ice sheets around the Plio-Pleistocene transition marks the beginning of a global cooling trend.

The most recent shift in the climate system is the transition from glacial-interglacial cycles dominated by obliquity, which last about 41 kiloyears (ky) to glacial cycles which last about 100 ky. This transitional phase lasts from about 1200 kiloyears ago (ka) to about 600 ka and is called the Mid-Pleistocene Transition, or MPT (Clark et al., 2006). Some studies conclude that the 100 ky power was rather abruptly introduced around 640 ka (Mudelsee and Schulz, 1997; Mudelsee and Stattegger, 1997). Other authors reported a more gradual increase in 100 ky power over the MPT (Park and Maasch, 1993; Tiedemann et al., 1994). The use of the LR04 benthic stack removed a large part of the regional variability and wavelet analysis of this stacked record showed that the increase of 100 ky power began around 1250 ka (Clark et al., 2006)

However this transition is not just an increase in duration and intensity of the glacial phase but marks the shift to ice sheets which are driven by strengthened feedback mechanisms (Schmieder et al., 2000; Clark et al., 2006). The MPT resulted in ice sheets surviving over multiple insolation maxima before ending in rapid termination events. The glacial to interglacial transitions before the MPT were more gradual with interglacials lasting longer and glacial phases lasting for a relatively shorter duration (Maslin and Ridgwell., 2005). The benthic oxygen isotope records of this interval shows more equal division between interglacial and glacial phases and is

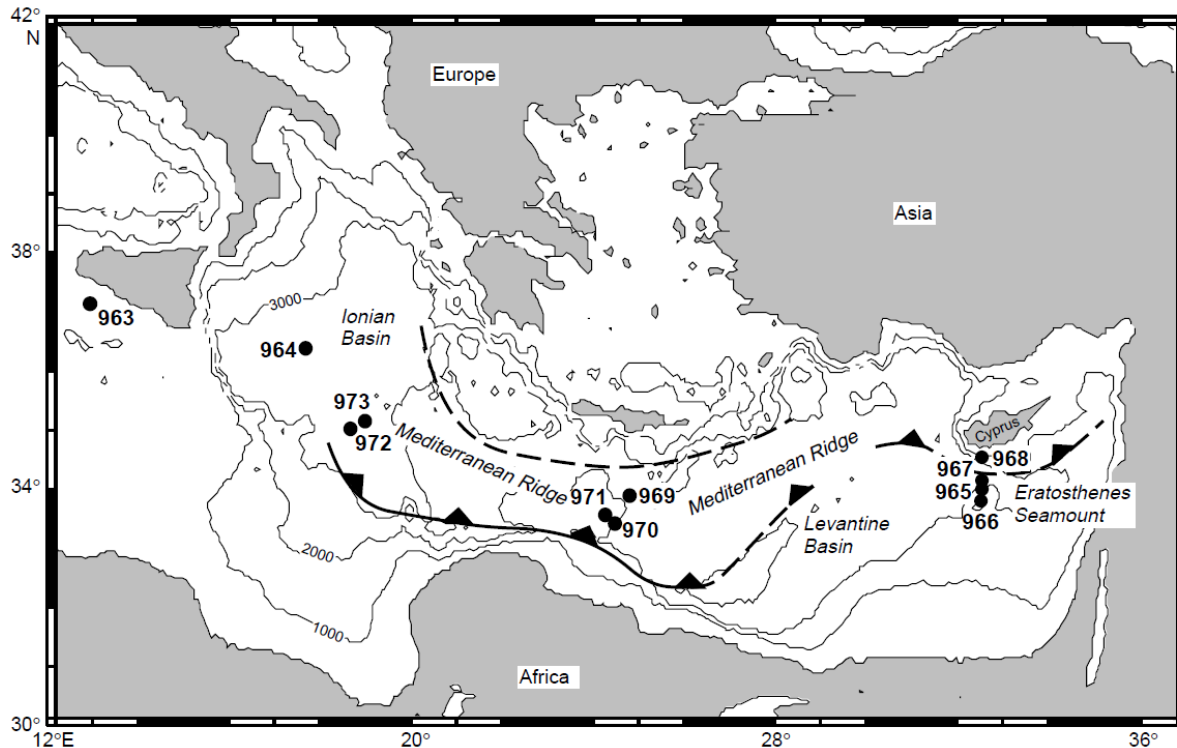


**Figure 1.** Map of the Eastern Mediterranean showing ODP site 967 to the south of Cyprus and the other drill sites visited during leg 160 of the Ocean Drilling Program. Figure adopted from Kroon et al. (1998).

therefore more in-line with the linear insolation forcing theory of Milankovitch (1941), which places the emphasis on obliquity controlled glacial cycles.

The Eastern Mediterranean ODP site 967 was chosen for its close location to the Nile delta while also recording the dust influx from North Africa during dry intervals (Figure 1). Using geochemical tracers as a proxy for North African climate an astronomical age model was constructed for this site, the workings of which are explained in § 2.3. The Mediterranean located at low intermediate latitude is ideally situated to record both the influence of precession as well as obliquity forcing. The MPT will be studied in the planktonic and benthic oxygen isotope records presented here, which covers the period from 1200 ka to 600 ka.

### *1.1. Possible mechanisms behind the MPT*

The MPT is seen as a shift away from the simple insolation forcing mechanisms to a more complex and nonlinear forcing of glaciation and deglaciation during the late Pleistocene (Maslin and Ridgwell, 2005). There are many theories to explain this shift in the global climate system and most of them focus on potential

enhancement of feedbacks or new feedback mechanisms which explain this nonlinear behavior, especially since there is no significant change in the astronomically controlled insolation forcing (Ruddiman et al., 1989; Imbrie et al., 1993).

Early work has focused on the seemingly similar length of glacial-interglacial cycles of the late Pleistocene and the 100 ky period of orbital eccentricity e.g. (Imbrie and Imbrie, 1980; Imbrie et al., 1993; Raymo, 1997). However since the direct effect of orbital eccentricity on insolation is very limited eccentricity alone cannot explain the observed variation. Other possible mechanisms have been explored. I will discuss some of the theories about the MPT below.

#### *1.1.1. Eccentricity forcing*

Shackleton (2000) attempts to explain the dominant ~100 ky cycle in ice volume and sea level. By stating that the 100 ky period in the benthic  $\delta^{18}\text{O}$  record lags behind temperature,  $\text{CO}_2$  and eccentricity. A benthic isotope record taken from the Pacific site V19-30 is compared with gas measurements from Antarctic Vostok ice cores. This atmospheric gas record is based on the air bubbles trapped in the Antarctic ice sheet. Shackleton (2000) argues that the  $\text{CO}_2$  concentration variations lead the nonlinear "ice volume" portion of the Vostok air  $\delta^{18}\text{O}$  and shows good coherence between these two. However the major variance at 100 ky is present in the atmospheric  $\text{CO}_2$  and the deep ocean temperature records, which both are in-phase with regard to eccentricity. This suggests that  $\text{CO}_2$  has had an immediate effect on the deep water temperature and air temperature (Shackleton, 2000). This in turn has affected the ice sheets. Although the processes through which orbital eccentricity could have forced changes in the atmospheric  $\text{CO}_2$  remain elusive (Shackleton, 2000).

#### *1.1.2. Obliquity control*

Huybers (2007) places the ~100 ky climate cycle in the framework of the 40 ky glacial-interglacial cycles of the early Pleistocene. He notes that the early Pleistocene (2-1 Ma) is dominated by obliquity, which controls the 40 ky climate cycles during this time. Huybers (2007) suggests that there is no single transition to increased 100 ky cyclicity over the MPT. Instead a gradual increase in the high latitude insolation threshold prior to deglaciation is proposed. Several physical processes which could explain the trend in the threshold value are proposed (Raymo,

1997; Clark et al., 1999; Tziperman and Gildor, 2003). The long term increase in threshold value over the Pleistocene meant that obliquity cycles are skipped more often in the late Pleistocene Huybers (2007). In addition if the accumulation of ice remained constant and glacial duration increases this could explain the saw-tooth character of these longer glacial phases.

#### *1.1.3. Cooling trend*

The gradual cooling over the Pleistocene is seen as a crucial part by many of the theories attempting to explain the MPT. One model, which relies on a slow cooling trend, is the sea-ice switch model of Tziperman and Gildor (2003). The model assumes a slow but steady cooling of the deep ocean over the Pleistocene. The cooling of the deep ocean reduces the temperature contrast between the surface and the deep ocean. This in turn allows for a more extensive and more rapid development of a sea-ice cover. The extensive sea-ice cover affects the ablation and accumulation of continental ice sheets. This thought to happen through the effect that sea-ice has on the exchange of energy between the ocean and the atmosphere, changed albedo and moisture availability (Tziperman and Gildor, 2003).

#### *1.1.4. Regolith hypothesis*

The regolith hypothesis states that the buildup of a larger volume of ice was made possible by the removal of the regolith, which initially covered the bedrock (Clark and Pollard., 1998). Through erosion by consequent ice sheets over the Plio-Pleistocene the base of the ice sheets encounter the high friction bedrock substrate which causes the flow of the ice sheet to slow down and allows for thicker ice sheets to develop. These thicker ice sheets presumably covered the same area as the thinner ice sheets that intermittently existed since the early Pleistocene (Roy et al., 2004; Balco et al., 2005). This explains how and why the increased ice volume was accommodated and survived. This model is one of the few models that does not rely on a cooling trend to work.

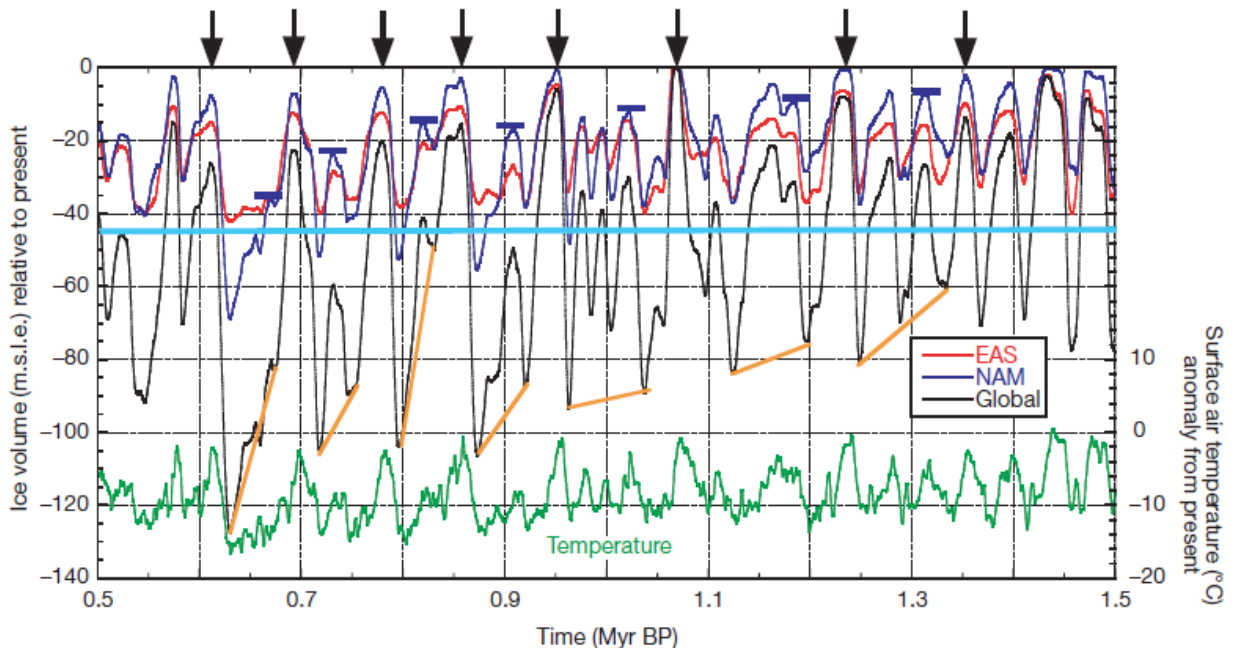


**Figure 2.** Modeled global ice volume (black), North American ice sheet (blue) and Eurasian ice sheet (red) all three are presented as meter sea level equivalent. The change in modeled surface temperature from the present (green). Figure adopted from Bintanja and Van de Wal (2008).

#### 1.1.5. Modeling ice volume

Bintanja et al. (2005) developed a model in an effort to separate the temperature and ice volume impact on the marine oxygen isotope record. They showed that ocean cooling is important during the early part of a glacial, later ice volume becomes the dominant part of the change in  $\delta^{18}\text{O}$ . Further work by Bintanja and Van de Wal (2008) focused on the emergence of the 100 ka climate variability. Model results of ice sheet volume showed that before the MPT the European ice sheet had the largest volume while after the MPT the North American ice sheet became dominant (Figure 2). A threshold in ice volume of the North American ice sheets of about 45 meter sea level equivalence is thought to have been reached around 900 ka (MIS 24) (Bintanja and Van de Wal, 2008). This threshold was reached due to the slow cooling of global climate since the end of the Pliocene (Bintanja and Van de Wal, 2008). Past this threshold, the ice sheets have grown large enough for the Cordilleran and Laurentide ice sheets to merge. This single larger ice sheet would then be more sensitive to climate feedback mechanisms when maximum ice volume is reached. This would also explain why the North American ice sheet grew larger while the European ice sheet did not.

## *1.2. Pleistocene data sets*

### *1.2.1. LR04 Benthic stack*

The LR04 benthic  $\delta^{18}\text{O}$  stack (Figure 3) is a combination of 57 benthic marine oxygen isotope records collected from the Atlantic, Pacific and Southern oceans. There are however only two sites which are located in the Indian ocean present in the LR04 stack. The LR04 covers a period from 5.3 Ma to present with a resolution of about 1-2 ky for the last 1.5 Ma. The location of the benthic isotope records used are distributed over different latitudes, longitudes and depths. One of the goals of stacking multiple benthic oxygen isotope records was to create a common timescale and to create a global standard for the paleoceanographic community to reference and compare their data with. The benthic stack created by Lisiecki and Raymo (2005) has become a template to which many other researchers compared their benthic  $\delta^{18}\text{O}$  records and which can be used as a dating tool for these sediment cores (Wegmann and Pazzaglia, 2009; Pollard and DeConto, 2009; Sigman et al., 2010)

The 57 benthic  $\delta^{18}\text{O}$  records were combined into one stacked record by aligning them using an automated graphic correlation protocol match (Lisiecki and Lisiecki, 2002) The stacked record was tuned to the Imbrie and Imbrie (1980) ice model, with constraints on the sedimentation rates as an additional age control.

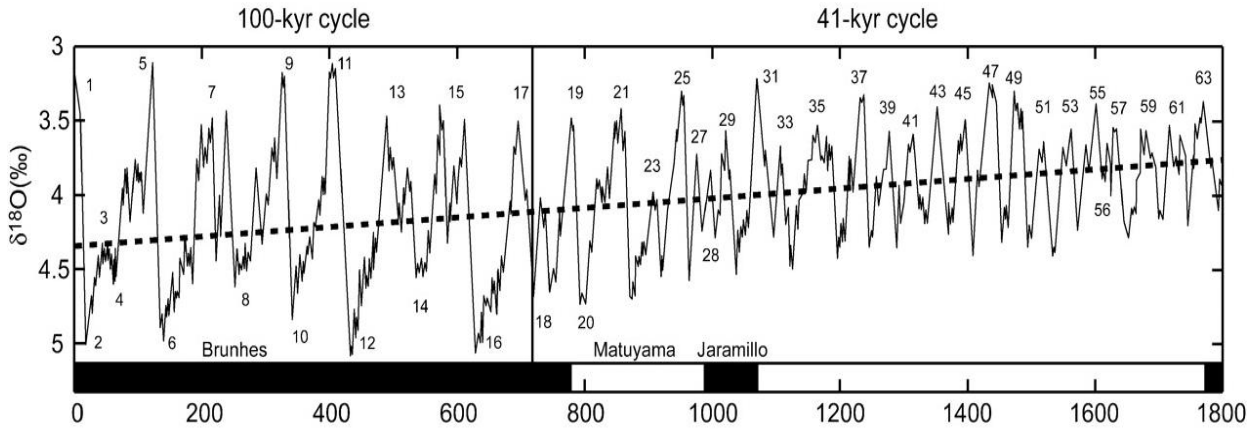


**Figure 3.** The stacked benthic  $\delta^{18}\text{O}$  record constructed from data sets collected from 57 sites globally. The dotted line indicates the linear trend, marine isotope stages are numbered. The magnetostratigraphic timescale shows the polarity reversals between chronos at the bottom of the figure. Figure adopted from Walker and Lowe (2007)

The age model used for the tuning was constructed by aligning the stack to a simple ice model based on the 21 June insolation at  $65^\circ\text{N}$ . This type of age model is claimed to be more reliable than an age model constructed from one or a few  $\delta^{18}\text{O}$  records. The tuning process concentrates mainly on obliquity by having the  $\delta^{18}\text{O}$  signal be in-phase with the obliquity component of the ice model. This is done because obliquity had the most influence on ice volume over the studied interval. The tuning target is based on the ice volume model first used in Imbrie and Imbrie (1980).

$$\frac{dy}{dt} = \frac{1 \pm b}{T-m}(x - y)$$

This formula which simulates ice volume ( $y$ ) through forcing by the 21 June insolation curve at  $65^\circ\text{N}$  latitude, represented by  $x$ . Term  $b$  is the nonlinear coefficient which is subtracted during ice growth and added during glacial terminations. This term determines if either glacials or interglacials become more pronounced and creates the sawtooth shape typical for late Pleistocene glacial cycles. The term  $Tm$  stands for the mean time constant and effects the amplitude between glacial and interglacials. For the youngest part a number of radiocarbon tie points were used, as was the Brunhes-Matuyama magnetic reversal at the beginning of the data set, as additional age control.

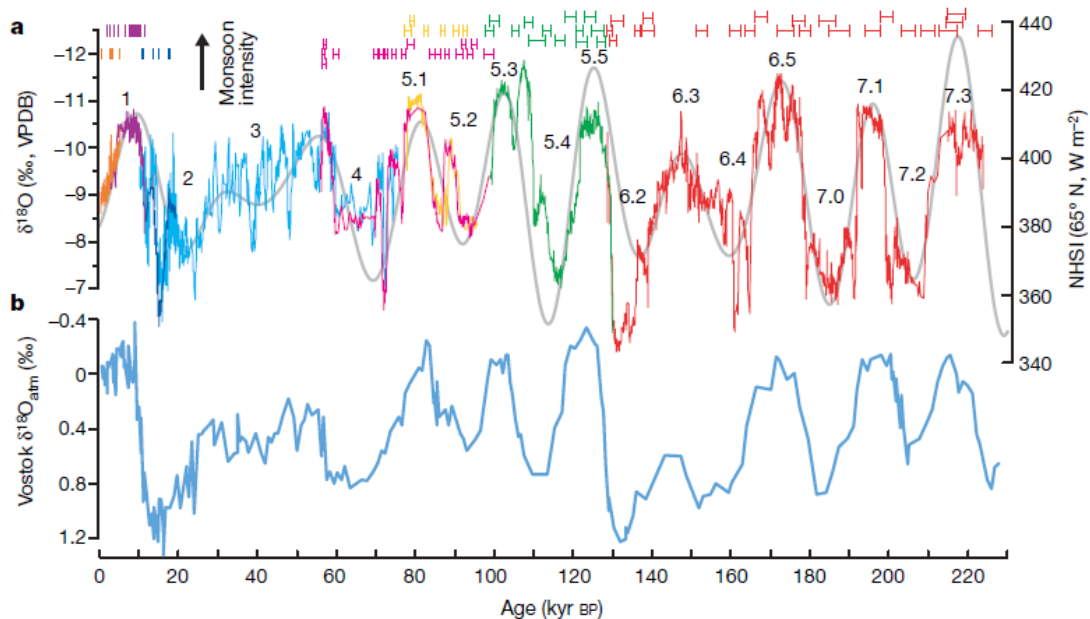


**Figure 4.** The top graph consist of several  $\delta^{18}\text{O}$  records collected from the Sanbao and Hulu cave stalagmites. The  $65^\circ\text{N}$  summer insolation curve is overlaid in gray. Marine isotope stages and sub-stages are indicated in the top graph. The bottom graph is the Vostok atmospheric  $\delta^{18}\text{O}$  record from Antarctica. Figure adopted from Wang et al. (2008)

A single benthic  $\delta^{18}\text{O}$  record contains more noise and the sedimentation rate is less constrained than with a stacked  $\delta^{18}\text{O}$  record. Lisiecki and Raymo (2005) assume that the global sedimentation rate was rather constant, from which they infer that their stacked record should also as a whole show little change in sedimentation rate. Errors in their age model would change the sedimentation rate of all their individual benthic records and such a global change in sedimentation rates is unlikely (Lisiecki and Raymo, 2005).

Some of the problems with the SPECMAP timescale are overcome by the LR04 timescale. The resolution has improved from on average 5 ky to 1-2 ky, which provides more certainty on the timing of glaciation and deglaciation and a more reliable analysis of phase relations. Since the LR04 uses a stacked benthic isotope record from a wide variety of locations it shows the effect of variation in global ice volume more clearly and no longer suffers from over pronounced precession driven temperature and salinity effects which affect surface waters.

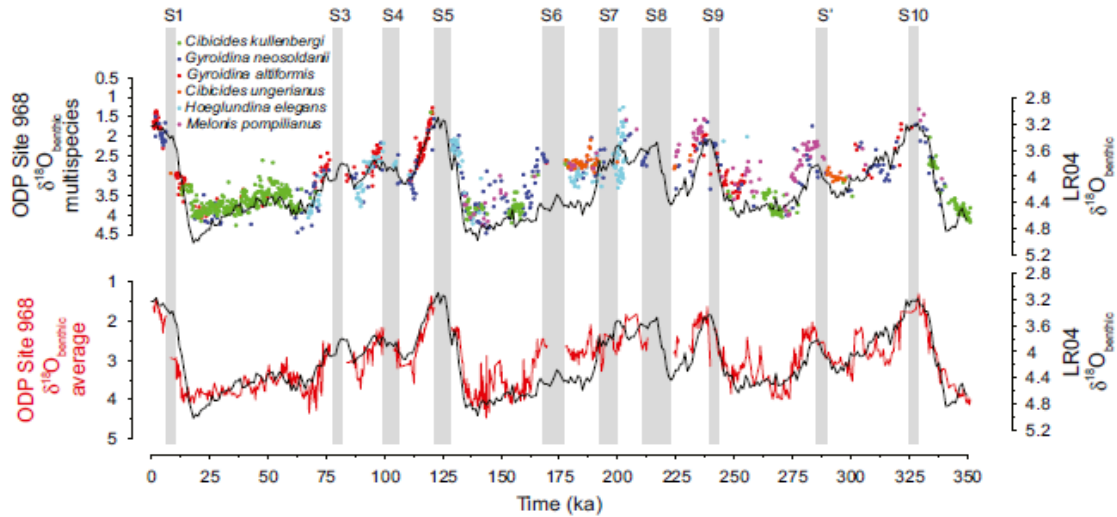


**Figure 5.** The top graph shows the individual  $\delta^{18}\text{O}$  measurements from ODP site 968 versus the LR04 benthic stack. The bottom graph shows the averaged  $\delta^{18}\text{O}$  values from ODP 968 versus the LR04 benthic stack. Sapropel layers are indicated by gray bars. Figure adopted from Ziegler et al. (2010).

### 1.2.2. Sanbao & Hulu cave timescale

The Sanbao and Hulu cave records consist of a  $\delta^{18}\text{O}$  record from stalagmites, indicative of East Asian monsoon activity. Absolute age control was achieved using  $^{234}\text{U}/^{230}\text{Th}$  radiometric dating (Wang et al., 2008). The dataset stretches back over the last 224 ka, covering the last two glacial cycles. Average resolution over the whole record is higher than 70 years (Figure 4). The oxygen isotope record shows a good match with  $65^\circ\text{N}$  summer insolation. The high resolution of the oxygen isotope record allows for an in depth analysis of millennial scale climate variability. Processes, such as Dansgaard-Oeschger cycles, seem to affect the timing of maximum summer monsoon intensity and have an effect on the phase relation between glacial termination and insolation forcing.

Ziegler et al. (2010) use the monsoon record from Wang et al. (2008) to refine the dating of Mediterranean sapropel layers from ODP site 968 (Figure 5). Monsoon proxies from site 968 such as the ratio Titanium to Aluminium and color reflectance show that the North African monsoon behaves very similar to the East Asian monsoon. Both records show similar millennial scale climate variability (Ziegler et al., 2010). This allows Ziegler et al. (2010) to use the absolute ages of Wang et al. through correlation of the respective monsoon proxies.

The paleoclimate record presented in Wang et al. (2008) is a high quality, high resolution climate record. Yet it is a monsoon climate record, not an ice volume record. For that we still need benthic oxygen isotope records. The relationship between maximum monsoon intensity and minimum precession established in Ziegler et al. (2010) can be used as a dating tool for an Eastern Mediterranean (Figure 5).

### *1.3. Aim of this work*

A comparison of the benthic record based on a Ti/Al age model used in this study to the widely used Lisiecki and Raymo (2005) LR04 benthic stacked record is aimed at exploring when both records differ and agree with each other. The LR04 record is based on astronomical tuning and assumes certain lags between ice sheets and astronomical cycles will be juxtaposed to the Ti/Al age model which does not directly tune the isotope record to astronomical cycles. The validity of the either age model will be assessed. The main uncertainties in the LR04 age model will be related to assumptions in the tuning parameters while the main uncertainties in the Ti/Al age model will be related to local effects on the timing of the Ti/Al peaks.

The benthic  $\delta^{18}\text{O}$  record will be used to determine the changes in ice volume over the studied interval. The planktonic  $\delta^{18}\text{O}$  record will be used to assess the local and regional influence as well as the effect of global climate variations on the Eastern Mediterranean. The results will be compared to studies which find comparable and opposing evidence and their interpretation of this data will be discussed.

### *1.4. Thesis setup*

**Chapter 2** describes the collection, treatment and analysis of the material collected from ODP site 967. The construction of the Ti/Al age model is also described in this chapter. Using the Ti/Al age model, which does not use astronomical tuning of the oxygen isotope record, allows for an independent comparison to other  $\delta^{18}\text{O}$  records. In addition independent investigation into the phase relation between ice volume and insolation forcing is made possible. In **Chapter 3** the oxygen isotope records will be presented. The major trends and characteristics will be described. Our isotope records will then be compared to the benthic  $\delta^{18}\text{O}$  stacked record of Lisiecki and Raymo (2005). This LR04 benthic  $\delta^{18}\text{O}$  record assumes a stable lag of the ice volume to insolation forcing for the middle and

late Pleistocene. This assumption will be tested using the Ti/Al age model and comparing the lag time of the benthic  $\delta^{18}\text{O}$  record from this study to the LR04 benthic  $\delta^{18}\text{O}$  record. The assumed lag time of ice volume to insolation is based on the most recent glacials, which have been thoroughly dated but are fundamentally different from the glacials before and during the MPT (Clark et al., 2006). Furthermore spectral analysis is performed on our  $\delta^{18}\text{O}$  records, characteristics and trends are discussed. Our benthic  $\delta^{18}\text{O}$  is tuned to a simple ice model by Imbrie and Imbrie (1980) and the results discussed at the end of chapter 3.

The MPT, as it is recorded in our oxygen isotope records, will be compared to other records in **chapter 4** (Mudelsee and Stattegger, 1997; Rutherford and D'Hondt; Lisiecki and Raymo, 2005; Elderfield et al., 2012). The evolution of climate will be placed in the existing framework of knowledge about the MPT, based on the best match with our data the most likely causes and effects will be discussed. The aim is not to solve the MPT "mystery". Instead I aim to construct a most likely series of events from Eastern Mediterranean perspective.



## 2. Methods

### 2.1. Materials

#### 2.1.1. ODP site 967

The sediment cores used in this study come from ODP leg 160, site 967, located in the Eastern Mediterranean (Figure 1). The site is located on the Northern slope of the Eratosthenes seamount, which is offshore and to the south of Cyprus, at 2554 meter below sea level (mbsl). The lithology of the cores is an alternation between bioturbated nannofossils ooze and nannofossil clay or sapropels (Kroon et al., 1998; Lourens et al., 2001). Occasional thin turbidites are present, however these are fine grained and have not disturbed the stratigraphic record (Konijnendijk et al., 2014).

#### 2.1.2 Stable isotope records

The benthic foraminiferal oxygen isotope record is based on the benthic genus *Gyroidina*, subspecies *neosoldanii* and *altiformis*. This epifaunal species has the highest abundance and was the most consistently present benthic species in the assemblage. In addition to the benthic record a planktonic foraminiferal oxygen isotope record was generated. Both the benthic specimens and the planktonic specimens were hand-picked from the size fraction  $>212\mu\text{m}$ . The planktonic samples were cleaned by putting them in vials with 98% ethanol and putting these vials in an ultrasonic bath for 2 seconds. After cleaning, the foraminifera were crushed and dried. The benthic and planktonic forams were analyzed with an automated carbonate reaction device (Kiel III) coupled to a Thermo-Finnigan MAT253. Each sample reacted with 103% phosphoric acid ( $\text{H}_3\text{PO}_4$ ) for 7 minutes at  $70^\circ\text{C}$ . Calibration to the international carbonate standard NBS-19 and in-house standard NAXOS were performed.

Part of the isotope data was already available and discussed in Konijnendijk et al. (2014). The data up until about 920 ka was available, the rest of the interval up until 1200 ka was collected for this study.

### 2.1.3. XRF

Bulk concentrations of major elements were determined by X-Ray Fluorescence (XRF). A few (3-5) grams from each sample were ground in a ceramic pestle and mortar which was cleaned with alcohol after each sample run. The ground samples were placed in a Leco TGA (Thermo-Gravimetric Analysis) to remove all residual moisture and oxidize organic matter and carbonates. This removal was achieved by heating the samples stepwise to five temperature stages (105, 450, 550, 800 and 1000° C respectively) until the weight of the sample stabilized. 600 mg of the residue was mixed with 6 g flux (a mixture consisting of 66% lithium tetraborate,  $\text{LiB}_4\text{O}_7$  and 34% lithium metaborate,  $\text{LiBO}_2$ ) and placed in platinum crucibles to which 0.500 ml of a 30% lithium iodide solution was added to prevent sticking of the molten sample to the crucibles. Subsequently the crucibles were placed in a Herzog Hag S automated fusion machine and fused to pearls. The pearls were measured in an ARL9400 X-ray fluorescence spectrometer twice, once for the major constituents like aluminium and iron and a second time on a more sensitive scale for minor constituents like zirconium barium. Analytical precision, as checked by parallel analysis of international reference material and in-house standards, is better than 1% for Si, Ti, AL, Fe, and better than 5% for Ba and Zr.

## 2.2. Geological background

The Mediterranean Sea is a semi-restricted basin, the Western end of which is connected to the North Atlantic and to the Eastern end connected to the Black Sea. Evaporation exceeds precipitation in the Mediterranean basin which results in the Mediterranean exporting warm and relatively saline water to the Atlantic. While in turn receiving relatively cold and less saline water, which flows in over the surface through the Gibraltar strait in a so-called anti-estuarine circulation. The result of this is that the Mediterranean is a so called nutrient desert because nutrients are lost through the outflow of deep water and no new nutrients are delivered by the surface current flowing into the Mediterranean basin (Robinson et al., 1991).

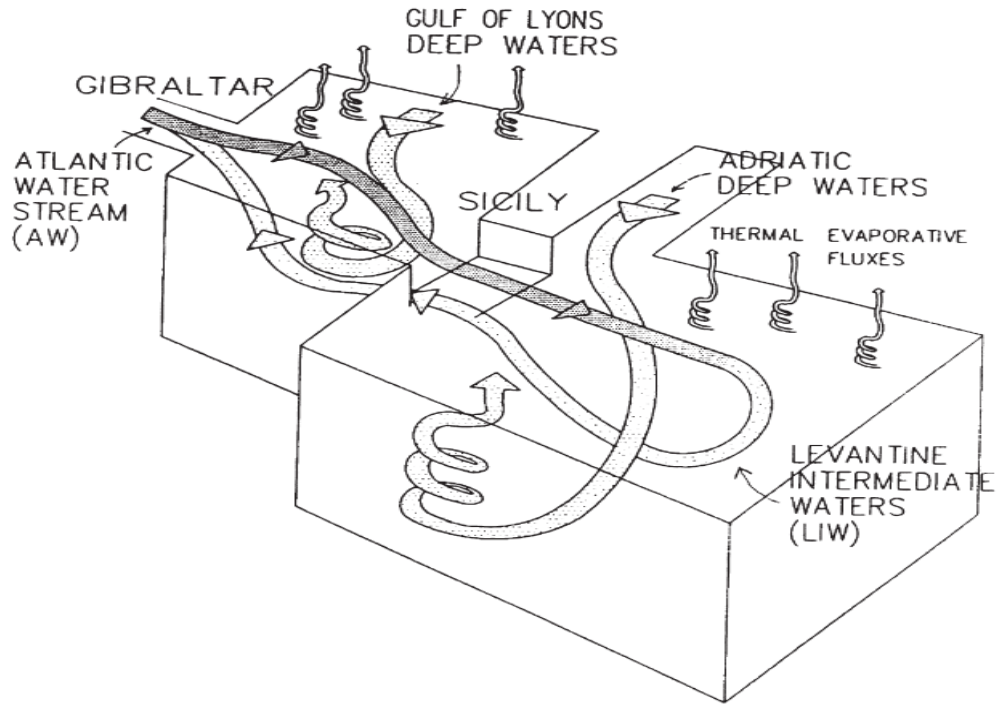


**Figure 6.** Schematic of the Mediterranean thermohaline circulation. Figure adopted from Lascaratos et al (1999)

The major locus of Mediterranean deepwater formation lays in the Eastern Mediterranean, specifically in the Adriatic and Aegean sea (Lascaratos et al., 1999). Here the water reaches the highest salinity through evaporation and the warm and saline water cools down during winter, becoming dense enough to form deepwater (Figure 6). The formation of intermediate water occurs in the Eastern Mediterranean with the Levantine Intermediate Water (LIW) being the major contributor to the Mediterranean outflow water (Lascaratos et al., 1999). The Eastern and Western sub-basins are separated by a shallow sill at the strait of Sicily. The LIW connects the deepwater of both basins since the Eastern Mediterranean deepwater is mixed and transported over the sill in the strait of Sicily and into the Western Mediterranean.

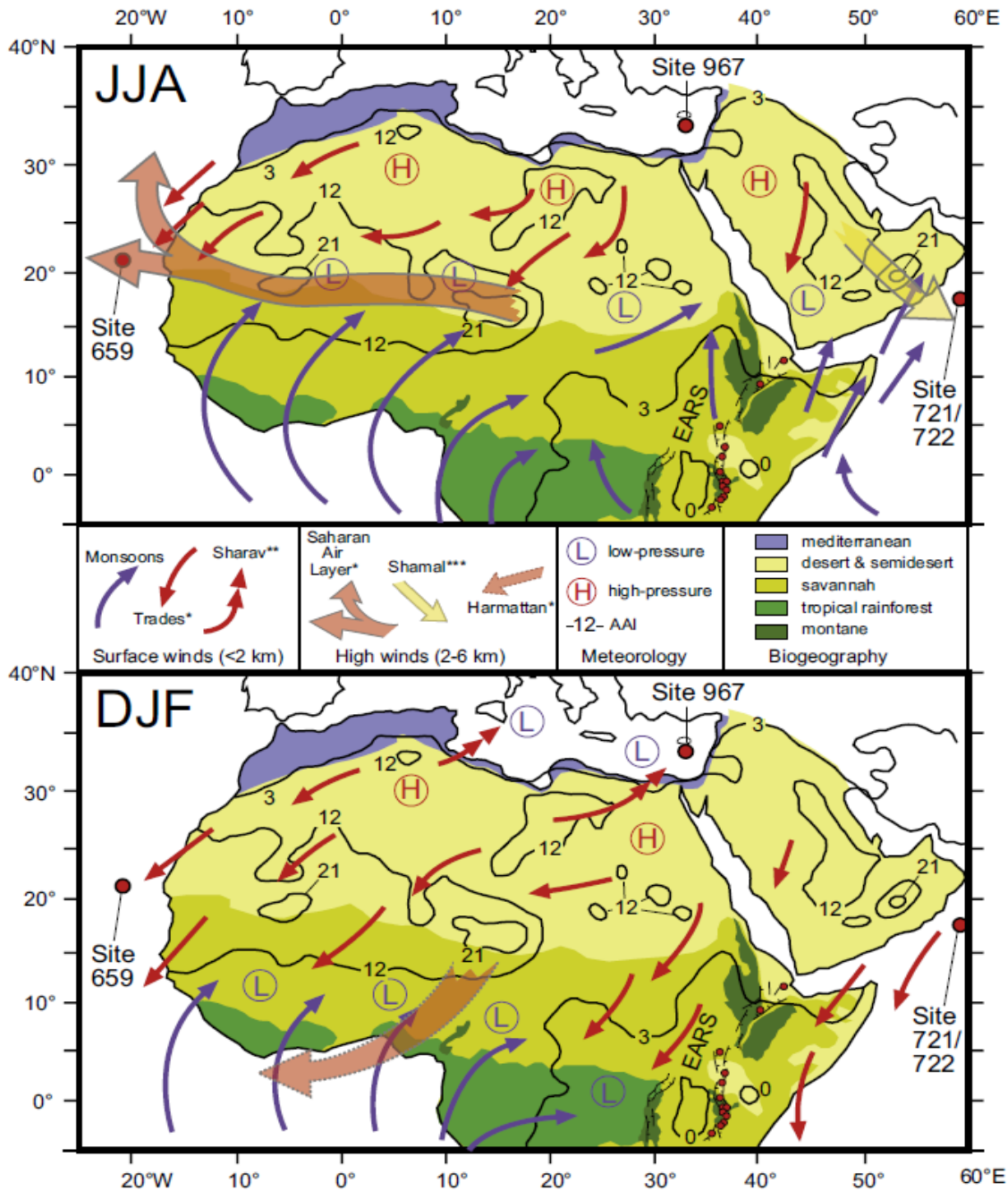


**Figure 7.** Map showing the location of ODP site 967. The top image shows the wind patterns during boreal summer. The bottom image shows the wind patterns during boreal winter. Figure adopted from Thrauth et al. (2009)

### *2.3. Ti/Al Age model*

The age model used in this study is based on the relationship between Titanium and Aluminum in the sediment. Most Aluminum in the sediment originates from clay minerals transported by rivers, in this case mainly the Nile river (Figure 1.) since this river is the major sediment supplier in the Eastern Mediterranean (Inman et al., 1984). Fluvial sediments containing Ti tend to be heavier and sink close to the river mouth (Wehausen and Brumsack, 2000). Therefore titanium is mainly supplied to the study area by aeolian processes such as dust storms that transport dust from the Saharan desert and arid parts of Northern Africa to the Mediterranean (Figure 7). High Ti/Al ratios are therefore indicative of more arid conditions over Northern Africa and low Ti/Al ratios are related to more humid conditions. These fluctuations from more arid to more humid conditions in the Saharan region are linked to the African monsoon (Jolly et al., 1998) and its ability to transport moisture into the interior of north African continent (Gasse, 2000).

Lourens et al. (2001) show the close link between Ti/Al ratio at ODP site 967 and variations in aeolian versus fluvial influence. The dust records from marine cores in West Africa and the Arabian sea show a complex relationship to insolation forcing and monsoon activity (Trauth et al., 2009) (Figure 7). This is because the transport mechanism of dust and the mechanisms that control dust production are related (Trauth et al., 2009). In contrast in the Eastern Mediterranean these two factors are unrelated, insolation forcing and monsoon activity are related to the Ti/Al ratio (Trauth et al., 2009). A detailed description of the tuning process can be found in Konijnendijk et al. (2014). The Ti/Al variations in the cores from ODP site 967 are linked to precession, where precession minimum is linked to a low Ti/Al ratio. This is because low precession is linked to a strong African monsoon and therefore a higher Al input to the sediment of ODP site 967. The age model thus generated is used to date the oxygen isotope record.

#### *2.4. Spectral analysis*

Spectral analysis of the benthic and planktonic oxygen isotope record was performed using the *analyseries* software (Paillard et al., 1996), which uses the Laskar et al. (1993) orbital solution. Fourier analysis was performed using the Blackman-Tukey method. Filtering of the planktonic and benthic records was centered on the frequencies peaks observed in the power spectrum of the respective records. The frequency range used to filter the records was approximately 20% of the filtered frequency. Cross correlation between the oxygen isotope records and 65°N 21 June insolation used the same Bartlett window and other parameters used in the Fourier analysis of the oxygen isotope records. Coherency between the oxygen isotope record and insolation is classified as significant at 80% and high at 90% coherency.

## 3. Results

### *3.1. Characteristics of the planktonic oxygen isotope record*

During rapid transitions between glacial and interglacial conditions, the Mediterranean overturning can slow down and dysoxic or anoxic conditions developed at depth in the Mediterranean basin, a process that results in the formation of an organic rich layer known as a sapropel (Rossignol-Strick, 1985). The planktonic  $\delta^{18}\text{O}$  record is almost continuous for the studied period, although there is a reduction in the number of planktonic foraminifera per sample during periods of sapropel formation (Figure 7), due to reduced preservation. The resolution of the planktonic  $\delta^{18}\text{O}$  record is about 1 ky over the total studied interval.

The planktonic  $\delta^{18}\text{O}$  record shows good correlation with the  $65^\circ$  North summer peak insolation (Figure 8). Every peak in insolation is matched by lighter planktonic  $\delta^{18}\text{O}$  values. However the amplitude of the  $\delta^{18}\text{O}$  variation does not seem linearly related to the strength of the insolation maximum. Some changes in the planktonic  $\delta^{18}\text{O}$  record are disproportionally large or small when compared to insolation as seen in figure 8, which is due to the simultaneous contributions of ice volume to the  $\delta^{18}\text{O}$  of ocean water and ice sheets on surface water temperature.

The lightest planktonic  $\delta^{18}\text{O}$  values measured in the studied interval are about  $-2.0\text{‰}$  with the heaviest  $\delta^{18}\text{O}$  value being around  $2.5\text{‰}$ . The  $\delta^{18}\text{O}$  values prior to 1 Ma are relatively stable, the amplitude variation in planktonic  $\delta^{18}\text{O}$  values hovers around  $1.5\text{‰}$ . The large peak during the interglacial around 950 ka (MIS 25) breaks this trend. While the subsequent interglacial  $\delta^{18}\text{O}$  values stay at the level before MIS 25 the glacial planktonic  $\delta^{18}\text{O}$  values become significantly heavier. This implies that SST's in the Eastern Mediterranean became colder during these glacial phases starting with the glacial phase around 900 ka (MIS 22). This interval has been called the "900 ka event" (Clark et al., 2006).

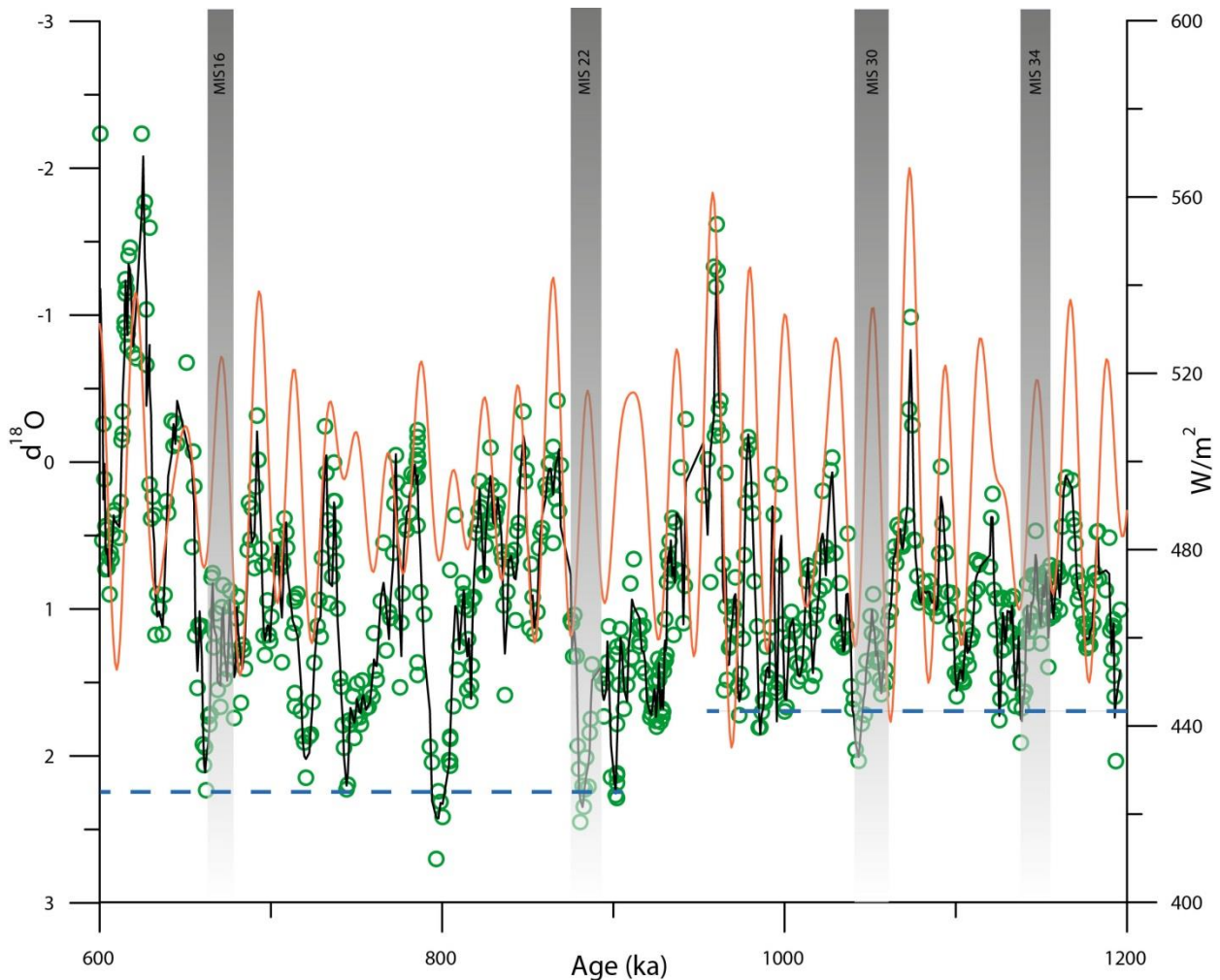


**Figure 8.** The 5 point moving average smoothed plankton isotope record from ODP site 967 (black), the unsmoothed data points are provided as reference (green circles). The 65°N June 21 insolation (orange) in  $W/m^2$ . The gray bands highlight periods when insolation was high but plankton isotopes remained heavy due to the cold conditions. Isotope stages are indicated for the highlighted glacials. The blue dashed line indicated the shift in average glacial plankton isotope values over the 900 ka event.

### 3.2. Characteristics of the benthic oxygen isotope record

During sapropel formation benthic foraminifera can disappear completely from the sediment record of site 967. The lack of data in some part of the record does not affect the overall pattern of the record. The benthic data set has an average resolution of about 2 ky over the total interval. The lightest  $\delta^{18}O$  value measured in the benthic record from the studied core is 1.0‰ with the heaviest  $\delta^{18}O$  value measured being  $\sim 4.4$ ‰.

The benthic record does not show the close coupling displayed in the planktonic record between  $\delta^{18}\text{O}$  and insolation (Figure 9). Not every peak in summer insolation is reflected by our benthic  $\delta^{18}\text{O}$  record since benthic isotope records are most sensitive to global ice volume changes and to a lesser degree temperature or salinity effects (Maslin and Ridgwell, 2005). Insolation peaks during glacial phases are often reflected in the benthic  $\delta^{18}\text{O}$  record as small excursions toward lighter  $\delta^{18}\text{O}$  values.

The mean  $\delta^{18}\text{O}$  value for the first half of the studied interval from 1250 ka to 900 ka is generally lighter than the interval after it, as shown in figure 9. Glacial terminations on average span a shift of  $\sim 1.5\text{‰}$  in  $\delta^{18}\text{O}$  during the early interval. The shape of the oxygen isotope curve resembles a square wave function, with long periods of light  $\delta^{18}\text{O}$  values during interglacial phases, especially up until 1 Ma.

The glacial  $\delta^{18}\text{O}$  values after 900 ka are significantly heavier than the full glacial conditions before the interval around 900 ka (Figure 9). Each glacial maximum after 900 ka until the end of the studied interval at 600 ka reach  $\delta^{18}\text{O}$  values heavier than about  $3.8\text{‰}$   $\delta^{18}\text{O}$  and most reach values heavier than  $4\text{‰}$ . Prior to 900 ka the benthic isotope values during glacial maxima only reaches  $3.5\text{‰}$   $\delta^{18}\text{O}$ .

The interglacial around 950 ka (MIS 25) marks a shift in the benthic  $\delta^{18}\text{O}$  values (Figure 9). Interglacial MIS 25 is marked by relatively light  $\delta^{18}\text{O}$  values that indicate a warm interglacial. The subsequent glaciation is marked by the heaviest  $\delta^{18}\text{O}$  values up until then at around  $4.2\text{‰}$ , almost  $0.8\text{‰}$  heavier than the average glacial before MIS 24. During the interglacial that follows (MIS 23) the  $\delta^{18}\text{O}$  values stay under  $3\text{‰}$ , indicating that a significant portion of the global ice volume must have survived the melting phase. The next glacial phase (MIS 22) records the heaviest  $\delta^{18}\text{O}$  values of the studied interval, with a maximum level of  $4.5\text{‰}$ . These two glacial phases around 900 ka are the glacial phases with the heaviest  $\delta^{18}\text{O}$  values which occur one after the other and the interglacial connecting them is coldest

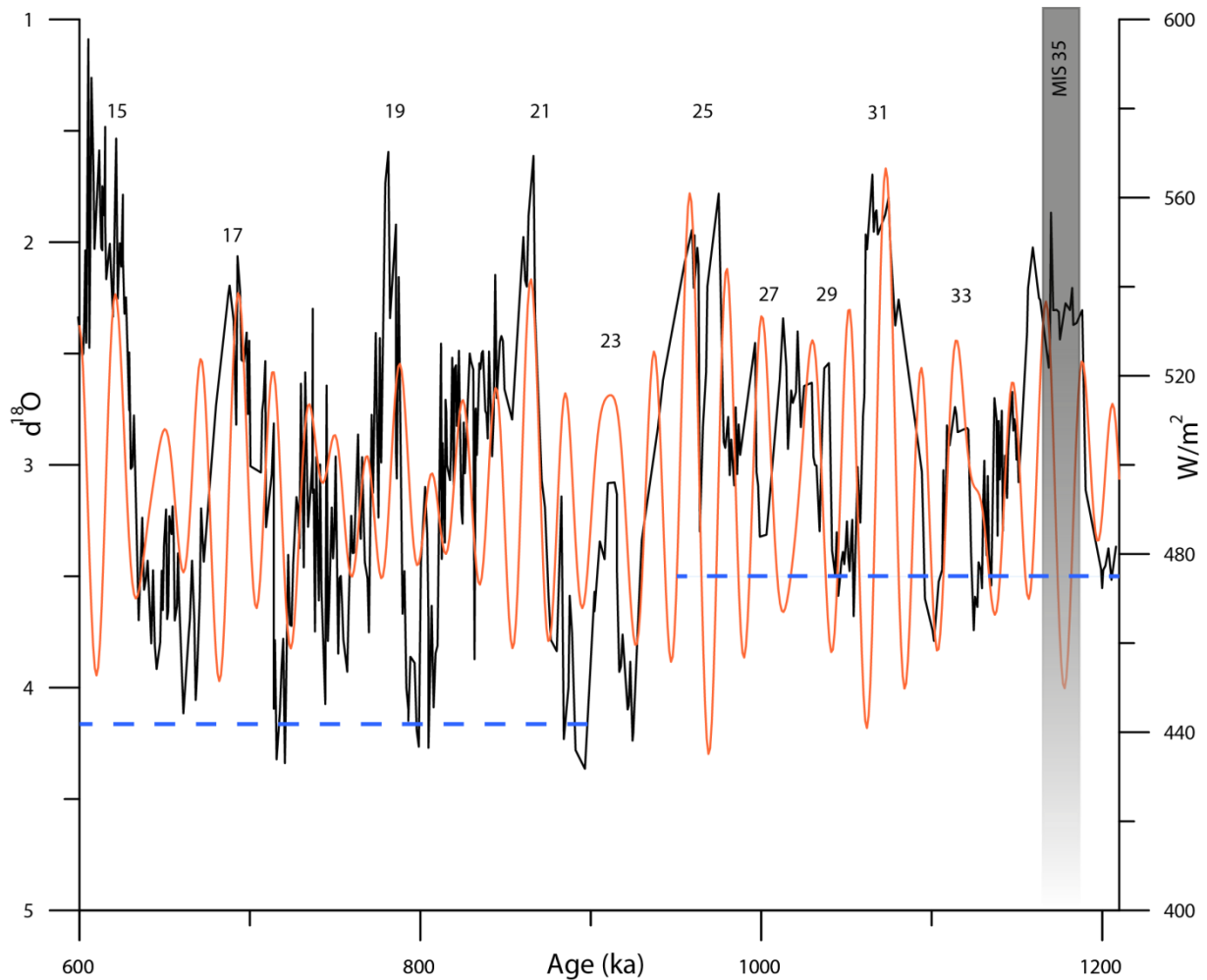


**Figure 9.** The benthic isotope record of ODP site 967 (black).65°N June 21 insolation (orange) in watt per meter squared. Marine isotope stages are indicated for the interglacial phases. MIS 35 is highlighted to indicate the anomalous relation with the insolation forcing. The dashed blue line indicates the shift in average glacial isotope values over the 900 ka event.

interglacial of the studied interval. That makes the interval MIS 25-21 a marked transition in the isotopic record. After the 900 ka event the character of the glacial-interglacial transitions is more sawtooth instead of the more square wave character dominant before 900 ka and glacial-interglacial amplitude grows to 2.5‰  $\delta^{18}O$ .

One notable exception to the good match between insolation and the isotope record occurs during MIS 35 which is highlighted in figure 9. The isotope reach interglacial conditions fast compared to the insolation forcing which to slightly lag the termination of MIS 36. The subsequent decrease in insolation seems to have no effect on the isotope record which remains at interglacial values for another 10 ky.

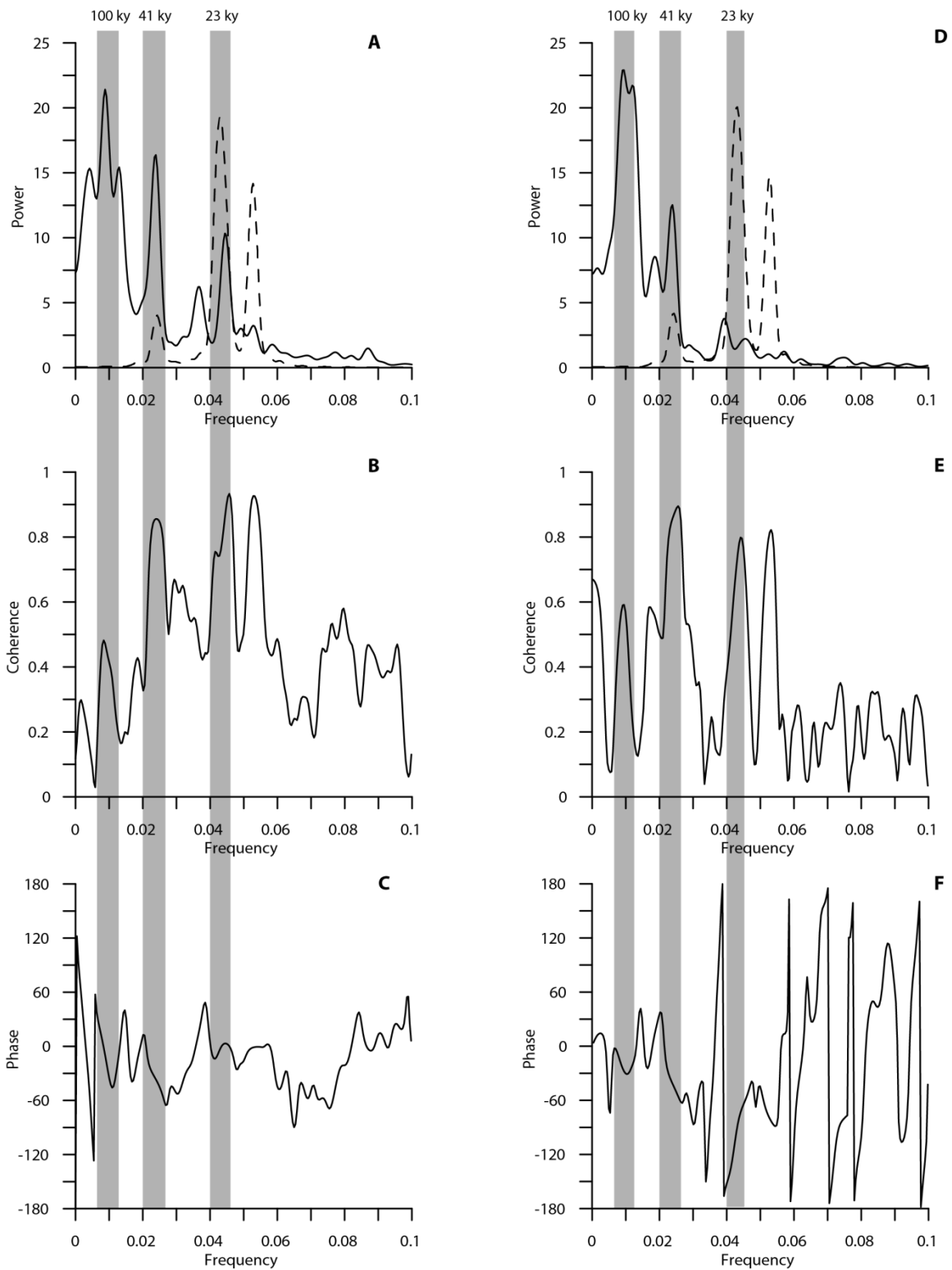


**Figure 10. a)** Power spectrum of the plankton isotope record, the main spectral peaks are indicated. **b)** The coherence between the 65°N June 21 insolation and the plankton isotope record. **c)** Phase between the 65°N June 21 insolation and the plankton isotope record, phases are in degrees with negative values indicating a lag and positive values indicating a lead of the plankton record compared to insolation. **d)** The power spectrum of the benthic isotope record, the main spectral peaks are indicated. **e)** The coherence between the 65°N June 21 insolation and the benthic isotope record. **f)** Phase between the 65°N June 21 insolation and the benthic record, phases are in degrees with negative values indicating a lag and positive values indicating a lead of the benthic record compared to insolation.

### *3.3. Spectral analysis of the oxygen isotope record of ODP 967*

#### *3.4.1. Planktonic $\delta^{18}O$ record*

The spectral analysis of the plankton record reveals a strong 23 ky signal which matches the 23 ky precession period in insolation (Figure 10a). The other major precession period with a period of 19 ky seems to be absent in our plankton record since there is virtually no power at this period. In addition to the absence of 19 ky power there is a small peak in the plankton power spectrum which reveals a 28 ky signal present in our record (Figure 10a). There is no orbital cycle with a 28 ky period in insolation although other researchers have found power at 28 ky in their records (Lourens et al., 2010). A large 41 ky signal is present which shows the obliquity influence on the plankton record of site 967 is strong (Figure 10a). The plankton record shows a dominant 100 ky signal with a shoulder around 80 ky in spectral analysis. The coherence between insolation and the plankton record is strong at 19 ky (Figure 10b) even though there is little power at this period (Figure 10a). There is high coherence for the obliquity and 23 ky precession orbital cycles. The 23 ky precession cycle is in-phase with regard to insolation while obliquity shows a small lag of  $\sim 3.5$  ky to insolation. The anomalous 28 ky signal shows a strange lead of  $\sim 4.5$  ky to insolation. However since there is no 28 ky cycle in insolation no conclusions can be drawn directly from this.

#### *3.4.2. Benthic $\delta^{18}O$ record*

The 19 and 23 ky precession periods are not present in the benthic isotope record (Figure 10d). There is an anomalous minor peak at 25 ky. Obliquity power is large with a minor peak at 54 ky. There is a major spectral peak from  $\sim 80$  to 100 ky present in the benthic isotope record. This wide range could reflect the combined eccentricity and double obliquity periods which may be important in this record. The absence of precession power notwithstanding a good coherence (figure 10e) between insolation and the benthic record is found at these periods (23 & 19 ky). Obliquity shows high coherency with insolation (Figure 10e). The anomalous 25 ky period seems to be in anti-phase with relation to insolation. The same anti-phase relation is prominent in low period ( $< 19$  ky) range (Figure 10f). The phase relation may be inaccurate for these periods due possibly to the lower data density of the benthic record. The obliquity signal lags insolation by approximately 3.5 ky which is about

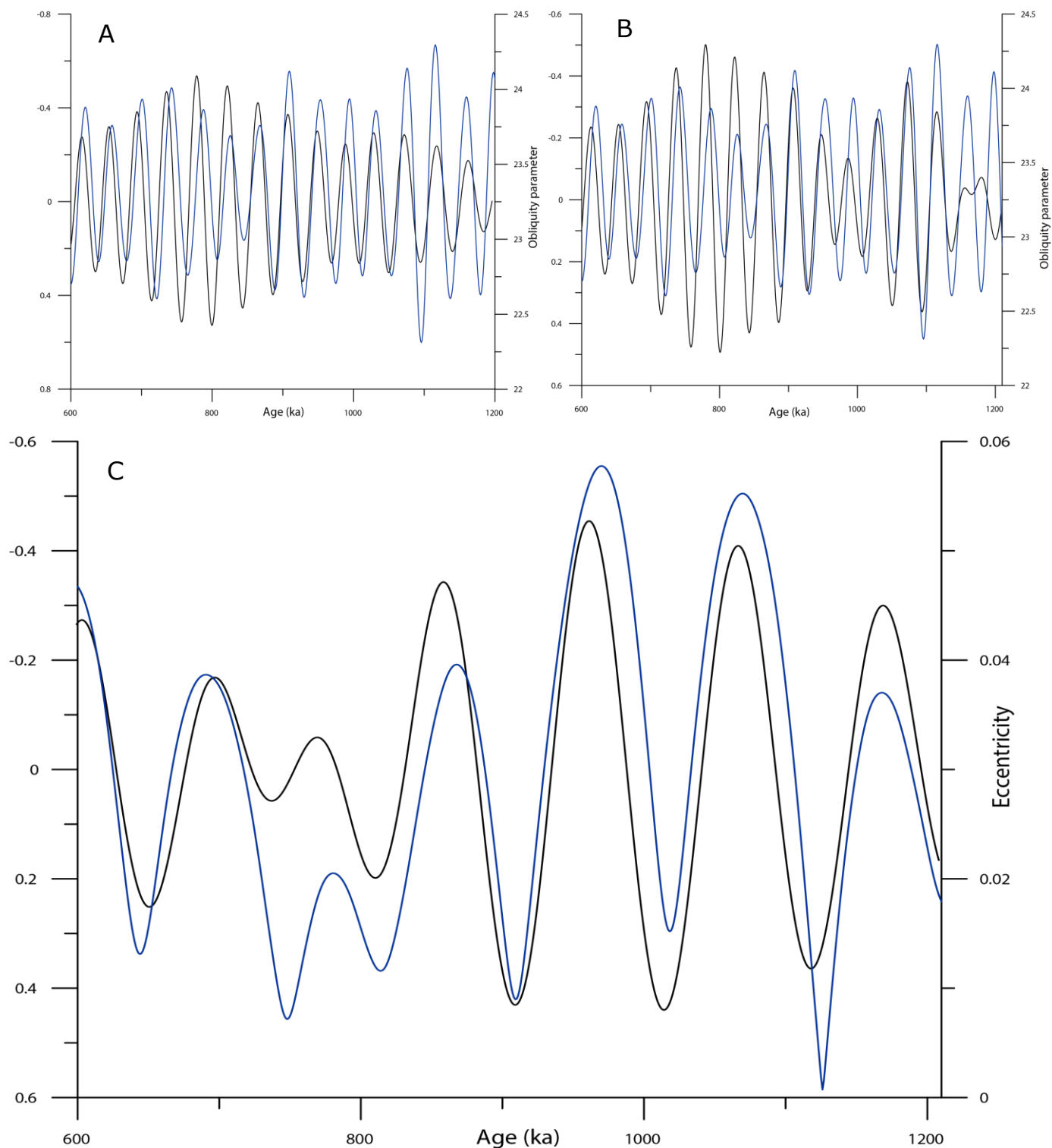


**Figure 11. a)** Filtered obliquity (41 ky) signal (black) from plankton record. Orbital obliquity parameter (blue), tilt in degrees. **b)** Filtered obliquity (41 ky) signal from benthic record (black). Orbital obliquity parameter (blue in degrees. **c)** Filtered eccentricity (100 ky) signal (black) from the benthic record. Orbital eccentricity parameter (blue).

the same lag that was found for the obliquity signal in the plankton record. An approximate lag of 4 ky was found for the wide 80-100 ky signal (Figure 10f).

#### *3.4.3 Filtered isotope records*

By filtering the obliquity signal at 41 ky from both the plankton (Figure 11a) and the benthic (Figure 11b) record trends in the phase relation can be found. The obliquity signal from both records is in-phase during the first half of the records. Towards the latter part both records show an increased lag of the filtered obliquity signal relative to the obliquity parameter (Figure 11a,b).

The filtered 100 ky signal from the benthic record matches orbital eccentricity well (Figure 11c). The amplitude oscillation of eccentricity can also be seen in the filtered eccentricity signal. This indicates that eccentricity modulation of precession is important in the benthic record. The 100 ky signal also lags eccentricity as suggested by the cross correlation of the isotope record and insolation (Figure 10f).

## 4. Discussion

### *4.1. Comparison of the ODP site 967 isotope record to the LR04 benthic stack*

The pattern of the ODP 967 benthic  $\delta^{18}\text{O}$  record can be easily correlated to the pattern in LR04. However there are some features present in the Mediterranean data set presented here that are not in the LR04 benthic  $\delta^{18}\text{O}$  stack and seem to be unique to the Mediterranean basin.

Compared to the change in  $\delta^{18}\text{O}$  value of 1‰ or less in the LR04 stack during glacial-interglacial transitions, the amplitude change is notably smaller than the average 1.5‰ amplitude recorded in the isotope record of site 967 (Figure 12). This is a local climate effect, due to the restricted nature of the Mediterranean basin (Rohling, 1994), whereas the LR04 record consists of open ocean records only (Lisiecki and Raymo, 2005).

This trend is described as well by Ziegler et al. (2010). They argue that due to the mechanism of deep water formation in the Mediterranean basin relatively warmer deep water is formed (Ziegler et al., 2010). The increased amplitude in benthic  $\delta^{18}\text{O}$  values in the Mediterranean indicates that there are local processes which amplify the contrast between glacial-interglacial cycles.

Some researchers argue that part of the amplitude variation in LR04 is removed as a result of the stacking method which reduces the regional effects and hence the amplitude of LR04 (Lisiecki and Raymo, 2005). Yet our benthic  $\delta^{18}\text{O}$  values are generally comparable to the values in the LR04 stack during glacial periods (Figure 12). The difference during glacial phases is quite small before 900 ka, no more than about 0.3‰. The difference during interglacials prior to 900 ka is between 1.0‰ and 0.5‰. The interglacial values after 900 ka differ by about the same margin as before 900 ka. The difference in glacial values decreases between our record and the LR04 record although for MIS 22 and 24 (~900 ka) the  $\delta^{18}\text{O}$  values of site 967 are significantly heavier than the  $\delta^{18}\text{O}$  values in the LR04 stack. The amplification is certainly strongest during interglacial phases when eccentricity is high. This would indeed suggest that precession, through the influence of the African monsoon, amplifies the interglacial  $\delta^{18}\text{O}$  values so they overshoot to much lighter

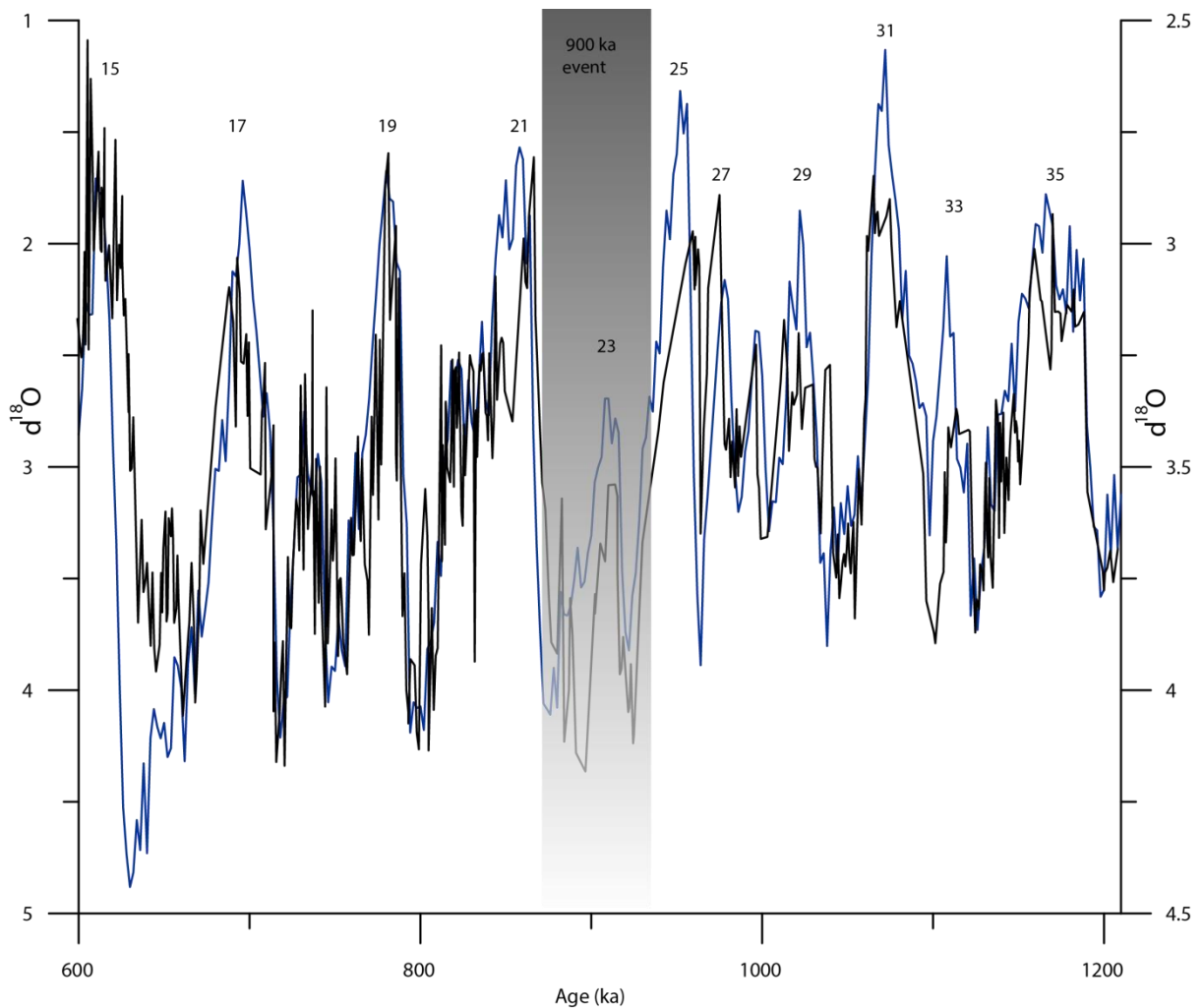


**Figure 12.** The benthic isotope record (black) of ODP site 967 plotted on the left axis. The LR04 benthic stacked record (blue) consisting of 57 records plotted on the right axis. Note the difference in scale between the two axis. The interglacial marine isotope stages are indicated.

values than the LR04 stack. One example to support this theory is MIS 33 which has a smaller absolute  $\delta^{18}\text{O}$  amplitude in ODP 967 compared to LR04. This is a reversal of the overshoot seen in the major glacial-interglacial transitions in the ODP 967 record. The eccentricity minimum which occurs at MIS 33 ensures the African monsoon's influence on the Mediterranean is weak and hence no amplification of benthic interglacial  $\delta^{18}\text{O}$  values occurs. Since all major glacial-interglacial transitions are linked to high eccentricity in the presented record they all show amplification compared to the LR04 benthic record.

The amplitude of the  $\delta^{18}\text{O}$  change from interglacial MIS 25 to glacial MIS 24 more than 2.0‰ while the amplitude variation over the same interval in the LR04 record is about half that value, at most. This indicates that significant amplification of the oxygen isotopes has occurred in the Mediterranean basin due to local climate effects. The heavy isotope values measured at 900 ka indicate the first full glaciation occurred around this time. This monsoon related amplification of interglacial phases in our record illustrates why the 100 ky period is so prominently present in ODP 967, although it is also dominant in the LR04 record.

The square wave character present in our record is best observed in our isotope record around 1120 ka (MIS 33). There is an increase to lighter  $\delta^{18}\text{O}$  values at the start of the termination, these lighter values persist for the next 10 ky, hence the MIS 33 resembles a square wave in our record. In the LR04 record the same trend can be seen. Other interglacials with a square wave character in our isotope record are MIS 35 and 31.

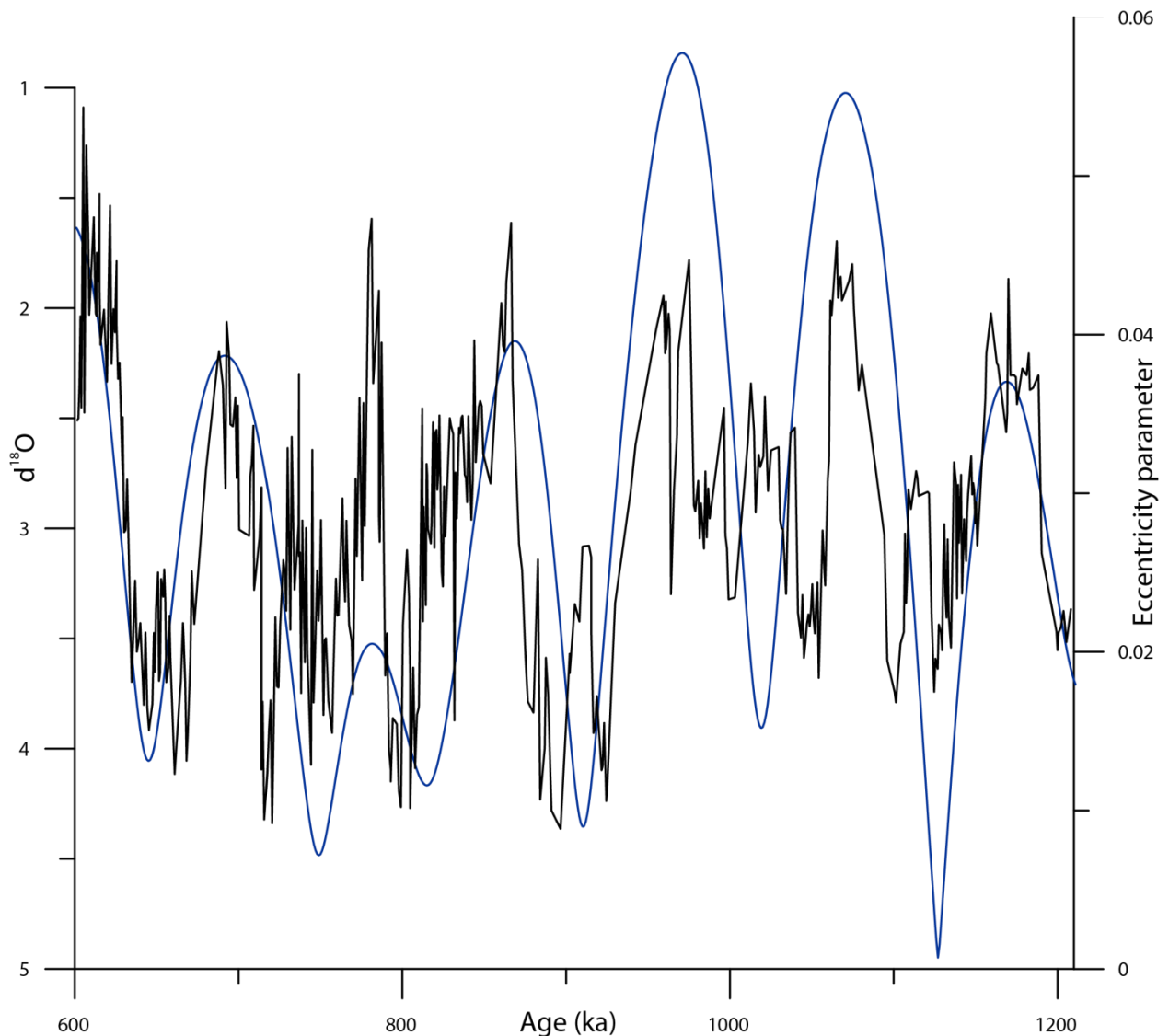


**Figure 13.** The benthic isotope record (black) of ODP site 967. The orbital eccentricity parameter (blue).

## 4.2. Onset of the MPT

### 4.2.1. The 100 ky climate rhythm and Eccentricity

A clear shift in the mean  $\delta^{18}\text{O}$  values is observed in the benthic oxygen isotope record around 900 ka. The characteristics of the isotope record before and after this shift differ. Therefore the early MPT or onset of the MPT will be discussed separately from the latter half of the MPT.

There is considerable power at the 100 ky period in the benthic record. This power seems to be present predominantly present from 1200 ka to 900 ka. Although some researchers have reported a later introduction of the 100 ky climate rhythm (Mudelsee and Schulz, 1997; Mudelsee and Stattegger, 1997) the work of Clark et al. (2006) showed this 100 ky cycle began around 1250 ka. Research done on

marine cores from tropical Africa (Jahn et al., 2005) indicate the start of the 100 ky cycle started around 1.6 Ma. Similar observation where made by Rutherford and D'Hondt (2000).

The interval between MIS 31 and MIS 25 show the highest amplitude 100 ky climate rhythm in the early MPT. Beginning at MIS 31 (~1072 ka), the termination leading up to this interglacial covers a relatively long period and is not sharp. The initial light  $\delta^{18}\text{O}$  excursion, after the glacial maximum of MIS 32, is triggered by a precession driven insolation maximum at 1094 ka. The subsequent insolation maximum at 1073 ka is synchronous with our benthic record reaching full interglacial values. This last insolation maximum was driven by the combination of a maximum in obliquity and a large minimum in precession. The precession amplitude is large due to a 100 ky eccentricity maximum. Low amplitude glacial-interglacial variations follow MIS 31. The next full interglacial is MIS 25 (~960 ka), which is again separated from the previous full interglacial by roughly 100 ky. High amplitude precession variation, in combination with high obliquity, drive a maximum in insolation. This maximum is similar in strength to the insolation peak at MIS 31. Again the insolation maximum seems to lead our benthic record by only a couple of ky, as was the case for MIS 31. The result is the strong presence of a 100 ky cycle in our benthic record. This 100 ky cycle corresponds to large amplitude variation in our benthic  $\delta^{18}\text{O}$  values.

The filtered 100 ky power from the benthic record shows good correlation to orbital eccentricity, both in amplitude modulation and phase. However the long duration of interglacial MIS 35, and to a lesser degree MIS 31, disturbs the record. The difference between the terminations, which precede these interglacials, is not 100 ky. The difference between the termination of MIS 35 and MIS 31 approximately 105 ky. The difference between MIS 31 and MIS 25 is ~120 ky. The midpoints of MIS; 35, 31 and 25 line up with the peaks in the 100 ky signal. Orbital eccentricity leads the filtered 100 ky signal by a couple of ky yet both the 100 ky signal and eccentricity lag the midpoint of the terminations preceding MIS 35, 31 and 25. Apparently eccentricity forcing plays some role in triggering these large deglaciation events, however the phase relation with the isotope record suggest direct insolation forcing by orbital eccentricity is unlikely.

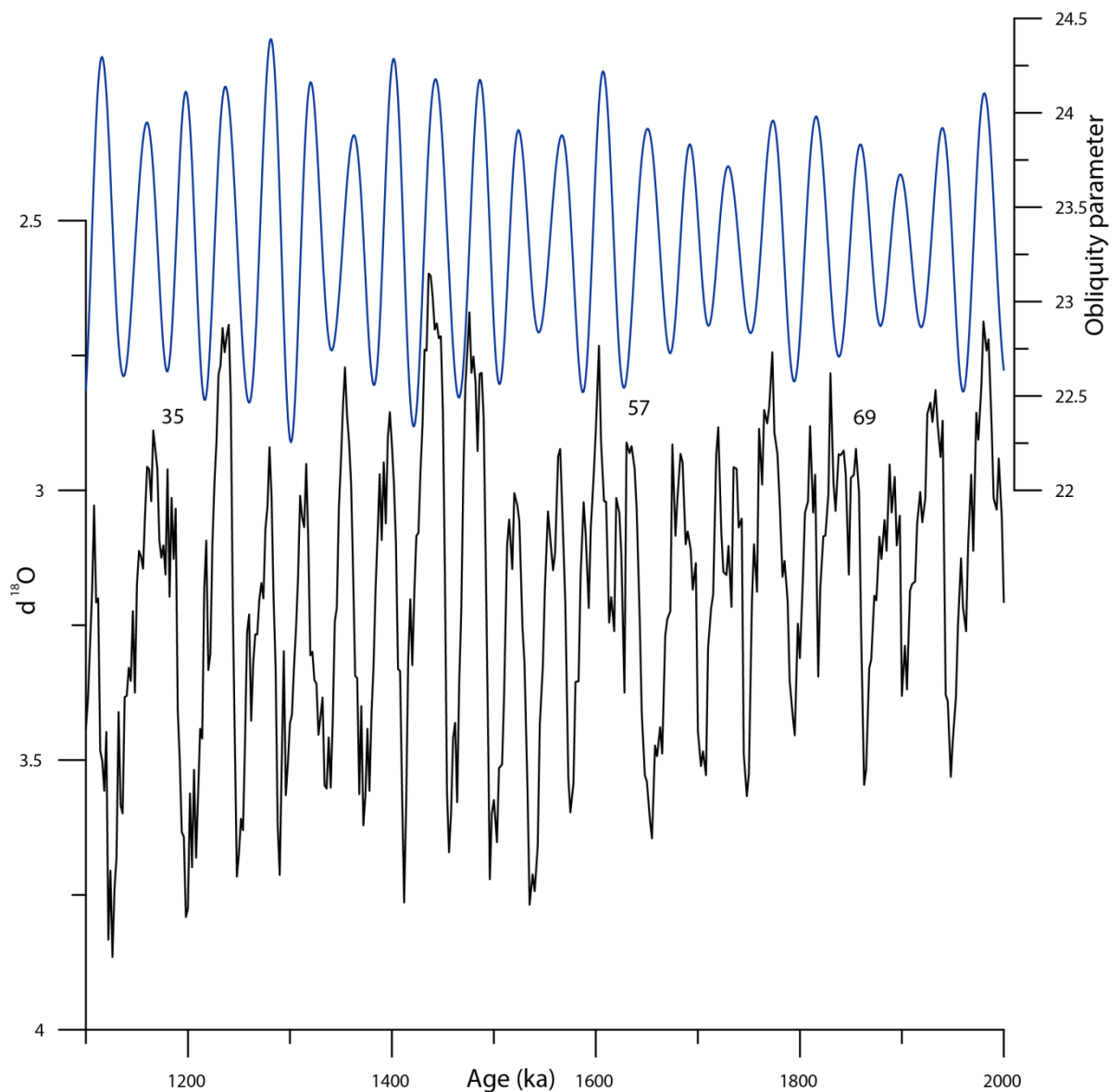


**Figure 14.** The LR04 stacked record (black) for the early Pleistocene (Lisiecki and Raymo, 2005). Obliquity (blue), tilt in degrees. Important isotope stage when obliquity was skipped are indicated.

#### 4.2.2. Obliquity and the skipping of the 40 ky period

The termination of glacial phase MIS 36 (~1205 ka), leading up to MIS 35, seems to have been triggered by precession forcing since orbital obliquity was decreasing at that time (Figure 14). The exceptionally long interglacial period that is MIS 35 covers almost 30 ky and resembles a square-wave. The filtered 41 ky period from the benthic record matches this square-wave character (Figure 11b) yet no such trend is observed in astronomical obliquity (Figure 11b). The orbital parameters of precession and obliquity don't show an extraordinary amplitude modulation around MIS 35, although there is an eccentricity maximum which is roughly synchronous with MIS 35. This skipping of obliquity minima has also been noted by Huybers (2007)

The termination prior to MIS 35, in our record and LR04, shows a lag of  $\sim 10$  ky to orbital obliquity. Due to the long duration of MIS 35 an obliquity maximum occurs at the end of this interglacial phase. By comparing the LR04 record to obliquity, from 1200 ka to 2000 ka (Figure 14), two comparable intervals are revealed. One occurs around 1650 ka at the start of MIS 57. The other starts around 1850 ka at the start of MIS 69. Both of these interglacials mark the start of a long period of light  $\delta^{18}\text{O}$  values. These intervals persisted over two obliquity maxima. MIS 35 is the last of such intervals, no comparable intervals are present until the end of the studied interval at 600 ka. The benthic isotope record does not record the obliquity minima during these intervals, there is no transition to a glacial stage. Instead light  $\delta^{18}\text{O}$  values persist and a long interglacial period is recorded

The interglacial MIS 33 ( $\sim 1120$  ka) is a relatively weak interglacial interval, which is forced by orbital obliquity. The midpoint of MIS 33 in our benthic record lines up with the maximum in orbital obliquity at 1115 ka. This implies an in-phase forcing relation of orbital obliquity to ice sheet melting for MIS 33. Insolation forcing is weak around MIS 33 and there is minimal amplitude variation in orbital precession. A 400 ky minimum in orbital eccentricity is centered at 1126 ka, which explains the low amplitude of orbital precession at 1120 ka. The 100 ky signal in our benthic record is at a minimum at 1114 ka (Figure 11c), this 100 ky signal lags the eccentricity minimum but is in-phase with the midpoint of MIS 33 in our record.

The abnormally long duration of MIS 35 caused midpoint of this interglacial to shift to an older age than expected. The skipped obliquity maximum before MIS 35 also assures there is no interference from a preceding interglacial. These factors ensure that the 100 ky signal lines up with the midpoints of MIS 35, 31 and 25. The eccentricity forcing does line up well with the filtered 100 ky rhythm (Figure 11c). There is a possibility that eccentricity forcing has contributed to the skipping of obliquity cycles in the isotope record observed around MIS 35. If so this occurred most likely through the modulation of the precession parameter, which in turn

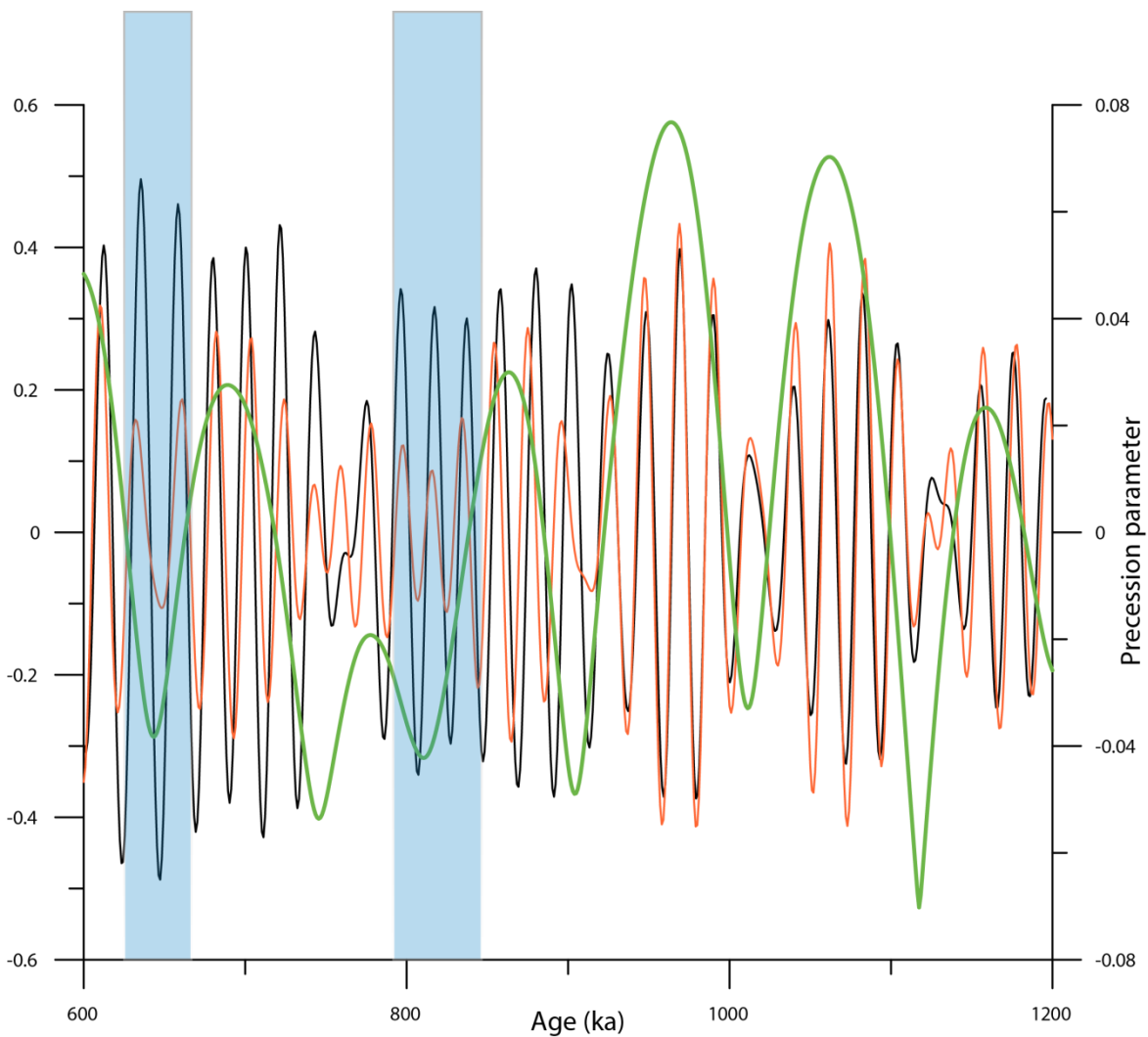


**Figure 15.** Filtered precession (black) from the plankton record of ODP site 967. The orbital precession parameter (orange). Orbital eccentricity parameter (green). The amplitude modulation of precession by eccentricity can be seen clearly in the orbital precession parameter. Anomalous modulation of the plankton precession signal is highlighted.

subdued the role of obliquity forcing. This suggests a stronger response of climate and especially ice sheets, to seasonal forcing, which is where most of the precession forcing power lies. The phase relation of eccentricity and the midpoints of the terminations preceding these large amplitude climate cycles is therefore of less importance since a sufficiently high precession modulation by eccentricity is required and not direct forcing through eccentricity.

#### *4.2.3. Precession and the 100 ky period*

The location of ODP site 967 in the Mediterranean means it ought to record the possible increase of eccentricity and precession forcing mechanisms on higher latitudes proposed by Rutherford and D'Hondt (2000). The clear precession signal at 23 ky in our plankton record does support the influence of precession forcing on surface water conditions. The influence of precession on surface conditions is expected but absent in the benthic record. Still eccentricity seems to be important in forcing large amplitude glacial-interglacial transitions. From our benthic record it is also clear that after the increase in glacial ice at 900 ka, combined high eccentricity and obliquity are needed to end a glacial period (Figure 9). Filtered precession from the plankton record is in-phase with orbital precession, the eccentricity modulation is also matched closely. However after about 900 ka the eccentricity modulation is disturbed in the plankton precession signal (Figure 15) while the in-phase relation with orbital precession remains intact. The perturbation in the plankton precession signal seems to be related to periods where obliquity is high after 900 ka. The amplitude in the isotope record at the precession scale remains high while actual precession forcing is decreasing (Fig 15).

### *4.3 Completion of the MPT*

#### *4.3.1. The 900 ka event*

After MIS 25 significant changes occur in our benthic record. Particularly the interval between 950 ka and 850 ka stands out. This second half of the record propagates the trends observed in the first half, like the phase relation with eccentricity. However the changes which occur around 900 ka in the isotope record add new trends.

Our benthic and plankton records both show signs of a shift in climate after MIS 25 (Figure 8 and 9). The glacials of MIS 24 and MIS 22 are regarded as the first increase of global ice volume since the start of the MPT (Bintanja et al., 2005; Sosdian and Rosenthal, 2009; Elderfield et al., 2012) Modeling results by Bintanja and Van de Wal (2008) suggest a maximum ice volume of more than 100 m.s.l.e. for MIS 22, comparable to the last glacial maximum (LGM) ice volume (Figure 2). Over the interval between MIS 25 and MIS 21 the single most significant shift in mean glacial  $\delta^{18}\text{O}$  occurs. The increase in ice volume explains the significantly heavier  $\delta^{18}\text{O}$  values yet the orbital configuration was not unlike the one during MIS 33.

The benthic  $\delta^{18}\text{O}$  values measured at MIS 24 and MIS 22 are the heaviest that were measured up until then. Even though there is an obliquity maximum in between MIS 24 and MIS 22 a full deglaciation is not achieved at MIS 23 (~915 ka). The amplitude of precession at MIS 23, at a 100 ky eccentricity minimum, is low. The orbital configuration resembles the one which occurred around MIS 33 (~1115 ka). In both cases deglaciation is initiated, paced by an obliquity maximum, yet full interglacial conditions are not achieved. The main difference between MIS 33 and MIS 23 is that the later occurs in between two much colder glacial stages than the glacial stages before and after MIS 33. There is no explanation for the increased cooling and the buildup of larger ice volume over the 900 ka event that can be found in direct insolation forcing.

#### *4.3.2. Combined precession and obliquity control*

The duration of glacial phases in our isotope after MIS 21 increased to ~80 ky. Glacial maximum  $\delta^{18}\text{O}$  values for MIS; 20, 18 and 16 are comparable to the heaviest  $\delta^{18}\text{O}$  values of MIS 24. The close coupling between variability in the benthic record, including glacial terminations, and obliquity continues. As does the eccentricity influence on the amplitude of the benthic record. The large amplitude glacial-interglacial cycles vary every second obliquity maximum, this also happens to be in-phase with eccentricity (Figure 13). The increased ice volume which is formed every ~80 ky after 900 ka changes the shape of the benthic isotope record to a more sawtooth like pattern. The weaker interglacial phases, in-between larger glacials, like MIS 33 and 23 don't seem to develop as fully. Although during MIS 18 there is a warmer phase which follows the same orbital format of MIS 33 and 23, low eccentricity during a relatively large obliquity maximum. Obliquity seems to be essential for the timing of terminations although the effect of obliquity forcing seems to depend more on the eccentricity controlled precession parameter to reach full deglaciation.

Comparable to the findings by Mudelsee and Schulz (1997) our record contains a ~80 ky climate cycle, after the increased ice volume of the 900 ka event. Contrary to Mudelsee and Schulz (1997) our benthic record already contained a ~100 ky climate cycle prior to the introduction of ~80 ky climate cycles. Yet the records of Mudelsee and Schulz (1997) and Schmieder et al (2000) suggest the 100

ky climate cycle is delayed until MIS 16. The effect of precession and eccentricity are already apparent in the record of site 967 before the shift in mean glacial isotope values around 900 ka. This implies that the climate system was already undergoing the effects that the increased influence of precession and eccentricity had before ice volume increased. Something that is also noted by Huybers (2011). After 900 ka the climate evolved, probably due to larger ice sheets and amplification of related feedback mechanisms, to a state where combined obliquity and precession forcing are required to terminate glacial phases.

#### *4.4. Causes of the mid-Pleistocene transition*

##### *4.4.1. Role of orbital forcing*

Before the 900 ka event the glacial ice volume did not increase significantly (Bintanja and Van de Wal, 2008). The large amplitude terminations reflect that, the increased amplitude is mostly due to lighter than usual interglacial  $\delta^{18}\text{O}$  hence warmer than usual interglacials. The influence that eccentricity modulation has, through precession, effects global climate significantly more than during the dominant 40 ky glacial cycles of the early Pleistocene (Tabor et al., 2014). The role of eccentricity modulation is therefore not only one of amplifying termination events but also one of suppressing the obliquity controlled 40 ky pattern in our record.

One option is that due to gradual cooling over the Pleistocene the insolation threshold of ice sheet melting increased, which increases the importance of precession and decreases the importance of obliquity (Huybers, 2006). This theory views the evolving sensitivity of ice sheets to obliquity forcing over the MPT as the product of a largely unchanged role of obliquity in pacing deglaciation. The cooling trend which is assumed by Huybers (2006) then results in an apparently anomalous increase in ice volume due to a higher melting threshold. However obliquity seems to completely lose the ability to force deglaciation after 900 ka, relying on the combination with high amplitude precession forcing to terminate glacials. Therefore the varying role of obliquity alone cannot explain the pattern observed in our data, eccentricity and precession forcing are integral to explain the changes observed over the MPT. There is no direct evidence for gradual cooling over the MPT (Hönisch et al., 2009) which means other mechanisms which are not reliant on cooling seem more plausible. To explain the ice volume increase at 900 ka several researchers have

looked into changes in ice sheet dynamics (Clark and Pollard, 1998; Clark et al., 2006; Bintanja and Van de Wal, 2008).

The 100 ky cycles, especially the sawtooth like transitions after 900 ka, must be viewed as the increase in hysteresis of the larger ice sheets. The increase in ice volume took place primarily on the North American continent (Bintanja and Van de Wal, 2008). As discussed in Abe-Ouchi et al. (2013) the hysteresis loop of the larger, North American, ice sheet allows for a more gradual change of ice sheet size for a large range of insolation forcings. This means that during the initial glacial phase, when higher eccentricity causes moderately large precession forcing, the still relatively small ice volume can maintain a positive mass balance. Over the rest of the glacial phase the ever decreasing eccentricity allows for the growth of the North American ice sheet over progressively smaller precession minima (Abe-Ouchi et al., 2013).

As can be seen in our data obliquity forcing cannot terminate these sawtooth like glacial intervals. Before 900 ka the pattern observed in our benthic record is not a sawtooth pattern and obliquity is able to force small deglaciations during low eccentricity hence MIS 33 and MIS 23 (Figure 13). This means that without higher glacial ice volume the role of eccentricity/precession is limited to a moderate increase in glacial-interglacial amplitude, mostly focused on lighter interglacial isotope values in our record. As discussed the LR04 stack shows less amplitude change before 900 ka which suggest that part of this increased amplitude observed in our data is due to local processes native to the Mediterranean. To explain the increase of ice volume over the 900 ka event changes in insolation forcing are not enough. Feedback mechanisms are the most probable forcing mechanism to explain the shift in glacial ice volume.

#### 4.4.2. Role of climate feedback mechanisms

A low latitude feedback on precession forcing is provided by monsoon intensification leading to increased methane levels (Loulergue et al., 2008). As observed in our Mediterranean record, increased monsoon influence triggered by high orbital eccentricity could explain the amplification seen in the isotope record of ODP 967. However if this was through greenhouse gas forcing this should effect the global climate. Because a similar amplification of interglacial  $\delta^{18}\text{O}$  values is not

observed in the global LR04 record (Lisiecki and Raymo, 2005) monsoon feedback mechanisms may not have a significant global impact. Still eccentricity power begins to enter into several benthic record's starting around 1200 ka (Clark et al., 2006).

If eccentricity modulation is forcing larger amplitude terminations some sort of threshold value is to be expected since the phase relation with the glacial terminations is so close that direct forcing seems unlikely given the phase relation of precession and obliquity forcing to the isotope record. At this threshold value of eccentricity modulation, precession forcing may be large enough to trigger a full termination. A threshold in precession forcing may be required for the African monsoon to extend it's influence farther to the North (Foley et al., 2003).

The binary nature of monsoon climate could therefore explain the threshold in precession forcing which requires a certain amount of eccentricity modulation. Greenhouse gas feedback at precession timescales can then be explained by the increased influence of monsoons on the production of these greenhouse gases. Also the role of vegetation feedback mechanisms must be considered, both at low latitude (Foley et al., 2003) and at high latitude (Tabor et al., 2014).

Although plausible the role of greenhouse gas feedback remains uncertain. More likely the ice volume is more sensitive to direct forcing of insolation by high precession amplitude (Abe-Ouchi 2013). Although Abe-Ouchi et al. (2013) does support some sort of threshold eccentricity modulation but relates it to unstable Northern Hemisphere ice sheets extending to the South. These ice sheets then, instead of greenhouse gas feedback being dominant, become more susceptible to precession forcing.

The increased influence of eccentricity modulation on glacial terminations observed in the LR04 record from the start of the MPT is amplified further in the Eastern Mediterranean. Most likely through increased monsoon impact coinciding with the new rhythm of glacial terminations which vary increasingly more at the pace of orbital eccentricity. The further southern extent of larger ice sheets after the 900 ka event makes them more susceptible to direct insolation forcing, primarily governed by precession (Abe-Ouchie et al., 2013). Since eccentricity was already

increasingly present prior to the 900 ka event this suggest a mechanism other than direct insolation forcing is responsible.

Abe-Ouchi et al. (2013) attributes the 100 ky glacial cycles to the unique behavior of the North American ice sheet. Bintanja and Van de Wal (2008) attribute the 900 ka event to the merging of the Cordilleran and Laurentide ice sheets. The merged North American ice sheet then grew thicker and extended further South (Bintanja and Van de Wal, 2008). These two theories show significant synergy in explaining the transition to longer glacial-interglacial cycles over the MPT, placing the emphasis on North American ice sheet dynamics.

To explain the increased eccentricity and precession influence before the merging of the North American ice sheets a different change in ice sheet dynamics can be considered. If the North American ice sheets began to extended further South prior to the 900 ka event they would become more sensitive to eccentricity modulated precession forcing. Such a change in ice sheet dynamics requires a change in surface conditions on the North American continent. This would contradict the premise of the regolith hypothesis (Clark and Pollard, 1998), which states that ice sheet became thicker as regolith was progressively removed from the continent. Without an increase in ice volume this would mean that prior to 900 ka the ice sheets could not have extended further South, according to the regolith hypothesis.

Another option is that the reconfiguration of the deep ocean circulation occurs (Siddall et al., 2010; Bates et al., 2014). They argue that the pacific deep water already approached freezing temperatures during glaciation at the start of the Pleistocene. Over the MPT the Atlantic and Indian deep water temperature stabilized around freezing temperature during glaciations (Bates et al., 2014). These stable deep water temperatures in all the ocean basins promoted the skipping of obliquity maxima until sufficiently high precession forcing caused a glacial termination (Bates et al, 2014). A controlling role for Antarctic sea ice extent on Antarctic deep bottom (AABW) is proposed. The extent of the Antarctic ice sheets to the edge of the continent around the time of the 900 ka event may have helped trigger this new extent of sea ice (Mckay et al., 2012). The strong production of AABW in turn decreases the north Atlantic deep water (NADW) formation, this promotes the formation of Northern Hemisphere ice sheets. A drawback is that a cooling trend has

to be assumed by Bates et al. (2014) for which little evidence exists (Hönisch et al., 2009).

Still it is conceivable that a sufficiently thinned regolith layer may have acted as a lubricant under the load of an ice sheet. During the final series of glacial cycles, before most regolith was removed, the dynamics of the ice sheet may have behaved in such a way as to promote more eccentricity and precession control over terminations.

#### *4.5. The Ti/Al age model, advantages and limitations.*

The Ti/Al age model suggests that part of the lag assumed in most orbital tuning of oxygen isotope records is unstable. This seems especially true for the period after 900 ka. The introduction of millennial scale variability, which increases over the MPT (Ferretti et al., 2010), doesn't seem to have increased the lag between obliquity forcing and climate response in our benthic record. Because our record was tuned independent of orbital cycles no specific astronomical period is artificially strengthened due to the tuning process.

Although the Ti/Al age model used in this study has benefits over direct orbital tuning of isotope records, it is heavily dependent on the location to be practically usable. The close link between the alternating arid and "green" North African source area of sediment and precession forcing of monsoon climate may not be unique, however these are quite specific conditions. The need for a wider range of dating methods for paleoclimate records over long timescales remains important, in that respect the Ti/Al is a powerful tool in the dating of Mediterranean paleoclimate data. Researchers should aim to develop new dating methods which are applicable globally over long timescales to gain new insight in past climate.

## 5. Conclusions

During the early part of the MPT the climate system already showed the presence of a 100 ky cycle in the benthic  $\delta^{18}\text{O}$  record of ODP 967. Similar precursor events have been observed during the MPT in climate records from low latitudes (Rutherford and D'Hondt, 2000; Jahn et al., 2005). The relatively small ice volume of the early MPT was evidently sensitive to exceptionally large insolation maxima driven by precession, but still paced by obliquity, resulting in complete deglaciation at the end of MIS 26, 32. Amplification of benthic  $\delta^{18}\text{O}$  values seem to be present from the start of the studied interval and is specific for the Mediterranean. The amplification is greatest during high eccentricity, which drives high amplitude interglacials to develop and lowest when orbital eccentricity is at a minimum. The role of eccentricity is important in the early MPT large amplitude glacial-interglacial transitions and becomes essential in the timing of deglaciation after the 900 ka event in combination with obliquity forcing.

The increased sensitivity of global climate to precession can be explained by a two-fold change in ice sheet dynamics. The increase in ice volume over the 900 ka event can be explained by a change in North American ice sheet dynamics. The merger of the two North American ice sheet dynamics proposed by Bintanja and Van de Wal (2008) explains the larger extent and volume. The increase in ice sheet sensitivity to precession is explained by Abe-Ouchi et al. (2013) "due to the gradual change between large and small equilibrium ice-sheet volume over a large range of insolation forcings" for the North American ice sheet (Abe-Ouchi et al., 2013).

The increased importance of eccentricity modulation before the 900 ka event is not linked to an increase in ice volume or insolation forcing. However a change in the way regolith covering North American continent interacts with the ice sheets may be envisioned while greenhouse gas feedback mechanisms remain elusive due to the lack of data.





## References

- Abe-Ouchi, A., Saito, F., Kawamura, K., Raymo, M. E., Okuno, J. I., Takahashi, K., & Blatter, H. (2013). Insolation-driven 100,000-year glacial cycles and hysteresis of ice-sheet volume. *Nature*, 500(7461), 190-193.
- Balco, G., Rovey, C. W., & Stone, J. O. (2005). The first glacial maximum in North America. *Science*, 307(5707), 222-222.
- Bates, S. L., Siddall, M., & Waelbroeck, C. (2014). Hydrographic variations in deep ocean temperature over the mid-Pleistocene transition. *Quaternary Science Reviews*, 88, 147-158.
- Bintanja, R., Van de Wal, R. S., & Oerlemans, J. (2005). Modelled atmospheric temperatures and global sea levels over the past million years. *Nature*, 437(7055), 125-128.
- Bintanja, R., & Van de Wal, R. S. W. (2008). North American ice-sheet dynamics and the onset of 100,000-year glacial cycles. *Nature*, 454(7206), 869-872.
- Clark, P. U., & Pollard, D. (1998). Origin of the middle Pleistocene transition by ice sheet erosion of regolith. *Paleoceanography*, 13(1), 1-9.
- Clark, P. U., Archer, D., Pollard, D., Blum, J. D., Rial, J. A., Brovkin, V., Mix A.C., Piasis N.G., Roy, M. (2006). The middle Pleistocene transition: characteristics, mechanisms, and implications for long-term changes in atmospheric pCO<sub>2</sub>. *Quaternary Science Reviews*, 25(23), 3150-3184.
- Coxall, H. K., Wilson, P. A., Pälike, H., Lear, C. H., & Backman, J. (2005). Rapid stepwise onset of Antarctic glaciation and deeper calcite compensation in the Pacific Ocean. *Nature*, 433(7021), 53-57.
- Elderfield, H., Ferretti, P., Greaves, M., Crowhurst, S., McCave, I. N., Hodell, D., & Piotrowski, A. M. (2012). Evolution of ocean temperature and ice volume through the Mid-Pleistocene climate transition. *Science*, 337(6095), 704-709.

Ferretti, P., Crowhurst, S. J., Hall, M. A., & Cacho, I. (2010). North Atlantic millennial-scale climate variability 910 to 790ka and the role of the equatorial insolation forcing. *Earth and Planetary Science Letters*, 293(1), 28-41.

Foley, J. A., Coe, M. T., Scheffer, M., & Wang, G. (2003). Regime shifts in the Sahara and Sahel: interactions between ecological and climatic systems in Northern Africa. *Ecosystems*, 6(6), 524-532.

Gasse, F. (2000). Hydrological changes in the African tropics since the Last Glacial Maximum. *Quaternary Science Reviews*, 19(1), 189-211.

Hönisch, B., Hemming, N. G., Archer, D., Siddall, M., & McManus, J. F. (2009). Atmospheric carbon dioxide concentration across the mid-Pleistocene transition. *Science*, 324(5934), 1551-1554.

Huybers, P. (2006). Early Pleistocene glacial cycles and the integrated summer insolation forcing. *Science*, 313(5786), 508-511.

Huybers, P. (2007). Glacial variability over the last two million years: an extended depth-derived age model, continuous obliquity pacing, and the Pleistocene progression. *Quaternary Science Reviews*, 26(1), 37-55.

Huybers, P. (2011). Combined obliquity and precession pacing of late Pleistocene deglaciations. *Nature*, 480(7376), 229-232.

Imbrie, J., & Imbrie, J. Z. (1980). Modeling the climatic response to orbital variations. *Science*, 207(4434), 943-953.

Imbrie, J., Berger, A., Boyle, E.A., Clemens, S.C., Duffy, A., Howard, W.R., Kukla, G., Kutzbach, J., Martinson, D.G., McIntyre, A., Mix, A., Molino, B., Morley, J.J., Peterson, L.C., Pisias, N.G., Prell, W.L., Raymo, M.E., Shackleton, N.J., Toggweiler, J.R., 1993. On the structure and origin of major glaciation cycles 2. The 100,000-Year cycle. *Paleoceanography* 8, 699-735.

Inman, D. L., & Jenkins, S. A. (1984). The Nile littoral cell and man's impact on the coastal zone of the southeastern Mediterranean. *Coastal Engineering Proceedings*, 1(19).

Jahn, B., Schneider, R. R., Müller, P. J., Donner, B., & Röhl, U. (2005). Response of tropical African and East Atlantic climates to orbital forcing over the last 1.7 Ma. *Geological Society, London, Special Publications*, 247(1), 65-84.

Jolly, D., Prentice, I. C., Bonnefille, R., Ballouche, A., Bengo, M., Brenac, P., ... & Waller, M. (1998). Biome reconstruction from pollen and plant macrofossil data for Africa and the Arabian peninsula at 0 and 6000 years. *Journal of Biogeography*, 25(6), 1007-1027.

Konijnendijk, T. Y. M., Ziegler, M., & Lourens, L. J. (2014). Chronological constraints on Pleistocene sapropel depositions from high-resolution geochemical records of ODP Sites 967 and 968. *Newsletters on Stratigraphy*, 47(3), 263-282.

Kroon, D., Alexander, I., Little, M., Lourens, L. J., Matthewson, A., Robertson, A. H., & Sakamoto, T. (1998). Oxygen isotope and sapropel stratigraphy in the Eastern Mediterranean during the last 3.2 million years. *Proceedings of the Ocean Drilling Program, Scientific Results*, Vol. 160; Chapter 14.

Laskar, J., Joutel, F., & Boudin, F. (1993). Orbital, precessional, and insolation quantities for the Earth from -20 Myr to +10 Myr. *Astronomy and Astrophysics*, 270, 522-533.

Lascazatos, A., Roether, W., Nittis, K., & Klein, B. (1999). Recent changes in deep water formation and spreading in the Eastern Mediterranean Sea: a review. *Progress in oceanography*, 44(1), 5-36.

Lisiecki, L. E., & Lisiecki, P. A. (2002). Application of dynamic programming to the correlation of paleoclimate records. *Paleoceanography*, 17(4), 1-1.

Lisiecki, L. E., & Raymo, M. E. (2005). A Pliocene-Pleistocene stack of 57 globally distributed benthic  $\delta^{18}\text{O}$  records. *Paleoceanography*, 20(1).

Loulergue, L., Schilt, A., Spahni, R., Masson-Delmotte, V., Blunier, T., Lemieux, B., ... & Chappellaz, J. (2008). Orbital and millennial-scale features of atmospheric CH<sub>4</sub> over the past 800,000 years. *Nature*, 453(7193), 383-386.

Lourens, L. J., Wehausen, R., & Brumsack, H. J. (2001). Geological constraints on tidal dissipation and dynamical ellipticity of the Earth over the past three million years. *Nature*, 409(6823), 1029-1033.

Lourens, L. J., Becker, J., Bintanja, R., Hilgen, F. J., Tuenter, E., Van de Wal, R. S., & Ziegler, M. (2010). Linear and non-linear response of late Neogene glacial cycles to obliquity forcing and implications for the Milankovitch theory. *Quaternary Science Reviews*, 29(1), 352-365.

Maslin, M. A., & Ridgwell, A. J. (2005). Mid-Pleistocene revolution and the 'eccentricity myth'. Geological Society, London, Special Publications, 247(1), 19-34.

McKay, R., Naish, T., Powell, R., Barrett, P., Scherer, R., Talarico, F., ... & Williams, T. (2012). Pleistocene variability of Antarctic ice sheet extent in the Ross embayment. *Quaternary Science Reviews*, 34, 93-112.

Milankovitch, M.M., 1941. Kanon der Erdbestrahlung und seine Anwendung auf das Eiszeitenproblem. Royal Serbian Academy, Belgrade

Mudelsee, M., & Stattegger, K. (1997). Exploring the structure of the mid-Pleistocene revolution with advanced methods of time-series analysis. *Geologische Rundschau*, 86(2), 499-511.

Mudelsee, M., & Schulz, M. (1997). The Mid-Pleistocene climate transition: onset of 100 ka cycle lags ice volume build-up by 280 ka. *Earth and Planetary Science Letters*, 151(1), 117-123.

Paillard, D., Labeyrie, L., & Yiou, P. (1996). Macintosh program performs time-series analysis. *Eos, Transactions American Geophysical Union*, 77(39), 379-379.

Park, J., & Maasch, K. A. (1993). Plio—Pleistocene time evolution of the 100-kyr cycle in marine paleoclimate records. *Journal of Geophysical Research: Solid Earth* (1978–2012), 98(B1), 447-461.

Pollard, D., & DeConto, R. M. (2009). Modelling West Antarctic ice sheet growth and collapse through the past five million years. *Nature*, 458(7236), 329-332.

Rohling, E. J. (1994). Review and new aspects concerning the formation of Eastern Mediterranean sapropels. *Marine Geology*, 122(1), 1-28.

Robinson, A. R., Golnaraghi, M., Leslie, W. G., Artegiani, A., Hecht, A., Lazzone, E., ... & Ünlüata, Ü. (1991). The eastern Mediterranean general circulation: features, structure and variability. *Dynamics of Atmospheres and Oceans*, 15(3), 215-240.

Rosignol-Strick, M. (1985). Mediterranean Quaternary sapropels, an immediate response of the African monsoon to variation of insolation. *Palaeogeography, palaeoclimatology, palaeoecology*, 49(3), 237-263.

Roy, M., Clark, P. U., Raisbeck, G. M., & Yiou, F. (2004). Geochemical constraints on the regolith hypothesis for the middle Pleistocene transition. *Earth and Planetary Science Letters*, 227(3), 281-296.

Ruddiman, W. F., Raymo, M., Martinson, D. G., Clement, B. M., & Backman, J. (1989). Pleistocene evolution: northern hemisphere ice sheets and North Atlantic Ocean. *Paleoceanography*, 4(4), 353-412.

Rutherford, S., & D'Hondt, S. (2000). Early onset and tropical forcing of 100,000-year Pleistocene glacial cycles. *Nature*, 408(6808), 72-75.

Tabor, C. R., Poulsen, C. J., & Pollard, D. (2014). Mending Milankovitch's theory: obliquity amplification by surface feedbacks. *Climate of the Past*, 10(1), 41-50.

Trauth, M. H., Larrasoaña, J. C., & Mudelsee, M. (2009). Trends, rhythms and events in Plio-Pleistocene African climate. *Quaternary Science Reviews*, 28(5), 399-411.

Tiedemann, R., Sarnthein, M., & Shackleton, N. J. (1994). Astronomic timescale for the Pliocene Atlantic  $\delta^{18}\text{O}$  and dust flux records of Ocean Drilling Program site 659. *Paleoceanography*, 9(4), 619-638.

Tziperman, E. & Gildor, H., (2003). Sea-ice switches and abrupt climate change. *Philosophical Transactions of the Royal Society of London. Series A: Mathematical, Physical and Engineering Sciences*, 361(1810), 1935-1944.

Schmieder, F., von Dobeneck, T., & Bleil, U. (2000). The Mid-Pleistocene climate transition as documented in the deep South Atlantic Ocean: initiation, interim state and terminal event. *Earth and Planetary Science Letters*, 179(3), 539-549.

Shackleton, N. J. (2000). The 100,000-year ice-age cycle identified and found to lag temperature, carbon dioxide, and orbital eccentricity. *Science*, 289(5486), 1897-1902.

Siddall, M., Hönisch, B., Waelbroeck, C., & Huybers, P. (2010). Changes in deep Pacific temperature during the mid-Pleistocene transition and Quaternary. *Quaternary Science Reviews*, 29(1), 170-181.

Sigman, D. M., Hain, M. P., & Haug, G. H. (2010). The polar ocean and glacial cycles in atmospheric CO<sub>2</sub> concentration. *Nature*, 466(7302), 47-55.

Sosdian, S., & Rosenthal, Y. (2009). Deep-sea temperature and ice volume changes across the Pliocene-Pleistocene climate transitions. *Science*, 325(5938), 306-310.

Walker, M., & Lowe, J. (2007). Quaternary science 2007: a 50-year retrospective. *Journal of the Geological Society*, 164(6), 1073-1092.

Wang, Y., Cheng, H., Edwards, R. L., Kong, X., Shao, X., Chen, S., ... & An, Z. (2008). Millennial-and orbital-scale changes in the East Asian monsoon over the past 224,000 years. *Nature*, 451(7182), 1090-1093.

Wegmann, K. W., & Pazzaglia, F. J. (2009). Late Quaternary fluvial terraces of the Romagna and Marche Apennines, Italy: Climatic, lithologic, and tectonic controls on terrace genesis in an active orogen. *Quaternary Science Reviews*, 28(1), 137-165.

Zachos, J., Pagani, M., Sloan, L., Thomas, E., & Billups, K. (2001). Trends, rhythms, and aberrations in global climate 65 Ma to present. *Science*, 292(5517), 686-693.